EXPERT SYSTEM FOR AERIAL VEHICLE DEPLOYMENT SYSTEM SELECTION

by

Lau, Ming Yui Edwin

BEng, Ryerson University, 2003

A report presented to Ryerson University

In partial fulfilment of the requirements for the degree of

Master of Engineering

In the Program of

~~Aerospace~~ Engineering

[Mechanical]

Toronto, Ontario, Canada, 2005

Author's Declaration

I hereby declare that I am the sole author of this report.

I authorise Ryerson University to lend this report to other institutions or individuals for the purpose of scholarly research

I further authorise Ryerson University to reproduce this report by photocopying or by other means, in total or in part, at the request of other institutions or individuals for the purpose of scholarly research.

Borrower's Page

Ryerson University requires the signatures of all persons using or photocopying this report. Pleases sign below, and provide address and date.

Abstract

An expert system is a programmable device developed to provide automation for engineering problem solving. It is composed of artificial intelligence modules, subroutine functions, and databases. Under this framework, a design process is proposed to assist the conceptual design of aerial vehicles' deployment systems. The problem is first defined by a set of design requirements for takeoff, landing, and cruise. The values are then translated to a set of performance parameters needed for the design process via a newly developed parametric search algorithm. Such parameters are categorised by a fuzzy inference module to determine the most suitable deployment-propulsion system, for conventional and V/STOL vehicles. Through the use of linear and neural network regression, a number of aerodynamic terms are estimated to support flight mechanics analyses, where the optimal takeoff and landing thrust vectors are determined. Engine specifications are deduced in terms of unit thrust, weight, bypass ratio and dimension. The design process demonstrates effectiveness in sizing engines for V/STOL operations.

Acknowledgement

The author thanks:

Emmett for his Civic,
Sam for his Skyline,
Andy for his AE86,
and Mom for her Accord.

Also:

Dr. Chung of Ryerson, Collegues of R.H.King, Victor of Jipolis and Winnie of Lidcombe.

Table of Contents

Nomenclature

a	=	acceleration, arbitrary parameter
b	=	arbitrary parameter
$\breve{c}_D$	=	minimum drag coefficient
$\breve{c}_L$	=	maximum lift coefficient
c_T	=	thrust coefficient
D	=	drag
d	=	diameter, largest cross section of engine
f	=	friction force
g	=	gravitational acceleration
L	=	lift
M	=	Mach number
m	=	mass
n	=	number of engines
P	=	power
S	=	wing planform area
T	=	thrust, of vehicle if unspecified
$\overline{T}$	=	thrust vector
t	=	time
v	=	speed, freestream if unspecified
W	=	weight, maximum takeoff if unspecified
x	=	instantaneous ground roll coverage
X	=	total ground roll
Z	=	altitude, service ceiling
β	=	bypass ratio
δ	=	degree of fuzzy membership
ε	=	error
Λ	=	configuration type
μ	=	coefficient of friction
ρ	=	air density
σ	=	aspect ratio
τ	=	thrust pitch angle
AI	=	artificial intelligence
D^2	=	deployment design process
E^3	=	expandable engineering expert system
V/STOL	=	vertical and/or short takeoff and landing, a general expression

All numerical values are expressed in standard SI units.

1 INTRODUCTION

The design of an aerial vehicle is an enduring process. From initial analysis to the integration of components, immense amounts of aeronautical knowledge related to theories and design histories are involved. In consideration of data compilation and extensive processing of decisions, the use of computation technology may provide an efficient method in aerial vehicle design. In this study, an expert system is developed as a software platform for the acquisition and application of aeronautical knowledge.

An expert system is the clustering of field specific knowledge, which provides decision making via the use of artificial intelligence, or AI. Expert systems are formulated to "simulate human expertise in a narrow domain" [1]. Applications of expert systems are found in many engineering design developments [2,3]. With the advancement of AI and the progressive reliability of individual engineering software, expert systems have evolved to centralise knowledge and provide the communication interface across software platforms [4,5]. This includes computer assisted design, simulation, database and optimisation algorithms. At the same time, due to their specialised problem solving nature, the transfer and reusability of knowledge are often limited. Individual system must then be modified or reconfigured to solve new or variants of the same problem. To construct a reusable expert system, it is necessary to establish an efficient framework for the organisation of knowledge, and to promote unrestricted knowledge acquisition capabilities. Consequently, large scale problems that require expert knowledge from different domains may then be solved, i.e., the design of aerial vehicles.

The term aerial vehicle broadly includes devices that are controllable during atmospheric flight including unmanned vehicles, utility props, jet transports, etc. Traditional airplane design first investigates all mission requirements and prioritises them accordingly. Once the design options are evaluated, components are fitted and sized based on such requirements [4]. Due to the breadth of airplane design knowledge, this study confines the problem of conceptual design by specialising in the selection of deployment propulsion system, i.e., for takeoff and landing. This is governed by the selection and thrust output of propulsion systems. Since the takeoff phase of a vehicle typically requires the maximum performance of engines, the resultant engine specifications are thus good measures of the general thrust requirements. This study investigates the performance domain of jet based deployment

systems. Conventional takeoff vehicles have thrust to weight ratio of about 0.4, and about 1.2 for vehicles with V/STOL capability. This demonstrates that the demand for thrust varies considerably depending on the deployment requirements [6,7]. In addition, the issues of thrust assisted lift, propulsive efficiency and vehicle stability need to be addressed in the layout and the sizing of engine units. As such, the design of deployment systems not only requires conventional airplane design knowledge [7], but also the development background of V/STOL vehicles [8].

Implementation of knowledge relating to the above into the expert system permits the use of AI towards the automation of mission requirement analysis systematically. Hence, this research aims to accomplish two goals:

1. Develop an expert system framework that is expandable, subject to solving various engineering problems. This framework is given the name of E^3.
2. Formulate a process of deployment design known as D^2, within the establishment of E^3.

This report first provides some insights of vehicle design specific to V/STOL. Then, towards the establishment of E^3, aspects of expert system are presented including the components of AI components. Utilising the resources of knowledge and expert system construction, the mission requirements of vehicles are fed into D^2 for analysis, and the final deployment system is proposed. Referencing to existing airframes, intermediate and final output results are validated in different perspectives for thrust based propulsion systems.

2 DEPLOYMENT DESIGN KNOWLEDGE

2.1 General Vehicle Design

New designs begin from a set of mission requirement, and are put forth to the conceptual phase of design. The phase analyses each of the design requirements and investigates the available design options. The available options are often categorised according to their structural or flight mechanics properties. For example, the selection of a wing involves characteristics like: tapered or elliptical, positive or negative dihedral, swept forward or backward, etc. These are determined from flight requirements and histories of related designs, i.e., numerical analysis and categorical data trend studies [7].

Similar literature relating to aerial vehicle design has classified knowledge is as follows [3]:

1. Governing knowledge: i.e., scientific laws and air traffic regulations.
2. Configuration knowledge: relating to individual components and the interactions among them.
3. Design process: solving the design problem efficiently.

The above descriptions of design knowledge are implemented into the subroutine and database modules of E^3 and are integrated into the process of D^2.

2.2 V/STOL Design

Since the 1950s, numerous V/STOL concepts, such as *'fan in wing'* and *'tilt wing'* have been tested [9,10,11]. Although many did not succeed to production developments, they have identified key areas to be overcome for the design of V/STOL vehicles:

- Thrust efficiency, as significant losses may incur upon the redirection of engine exhaust
- Integration of airframe and power plant, influencing the structural and flight dynamics of a vehicle
- Stability and control, particularly at low speed and during the transition from lift to cruise thrust

The progress of V/STOL research was profoundly driven by the need for carrier based operations. This is demonstrated by the production of the Yak-38 and the Yak-41 [10]. Later, the AV-8 and the F-35B of Figure 1 provide definite roles in naval operations.

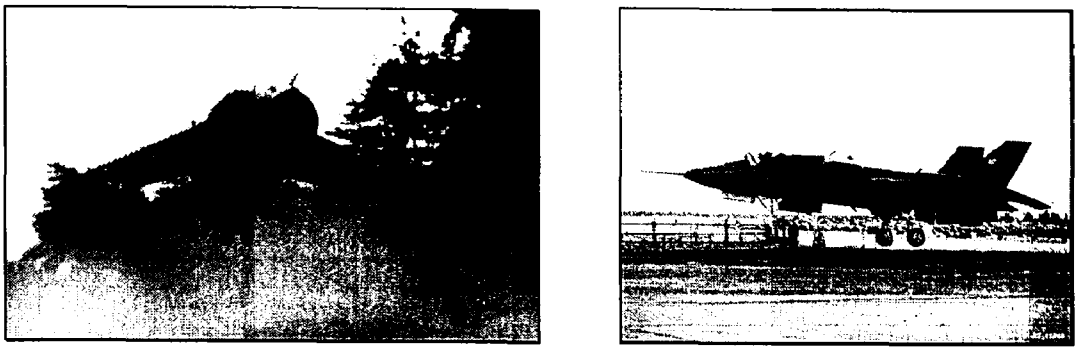

Figure 1: AV-8 [12] and F-35B

In addition, due to the high temperature and the high velocity of engine exhaust gas, jet V/STOL designs must properly address the following ground induced phenomena [8]:

- Recirculation of high temperature exhaust into the induction system, reducing the thrust performance of engines
- Generation of a low pressure region beneath the vehicle from the high velocity exhaust, such that the vehicle experiences a suck down effect
- Secondary lift effect from the rebound of exhaust gas from the ground

It was later realised that the high fuel consumption rate during the phase of vertical deployment has significantly limited the vehicle's mission effectiveness in aspects such as speed and payload capacity. This gives rise to the concept of short takeoff and landing systems. Most short takeoff designs originated from modifications of production designs. For example, the C-1 transport was converted to the Aska research aircraft with the takeoff lift provided by upper surface blowing of engine exhaust [13]; and mechanical thrust vectoring nozzles were equipped on the research models of the F-15 and the F/A-18 [14]. Throughout such dynamic history of V/STOL research, there are several types of deployment systems that demonstrated mission effectiveness and production feasibility. The following is a discussion of the six configuration types, in which some posses both conventional and V/STOL capabilities.

The *helicopter* rotor system is fundamentally designed for vertical takeoff. This configuration is referred to as $\Lambda = H$, where Λ is a variable expressing the configuration type. Since the rotor is aligned with to the vertical axis of the vehicle for lift thrust, the forward speed is generally limited within the low subsonic regime. Due to the relative size of the rotors, thrust is produce by providing momentum to a large mass flow. Consequently, helicopters' rotor systems have the highest propulsive efficiency among other propulsion types.

The *tiltprop* configuration, $\Lambda = P$, describes general propeller driven vehicles with emphasis on thrust pitch mechanism from 0° to 90° that enable V/STOL operations. Figure 2 is a layout of such production design featuring the V-22 Osprey. This configuration portrays both the vertical takeoff capability helicopters and the efficiency of propellers for mid subsonic flight [8].

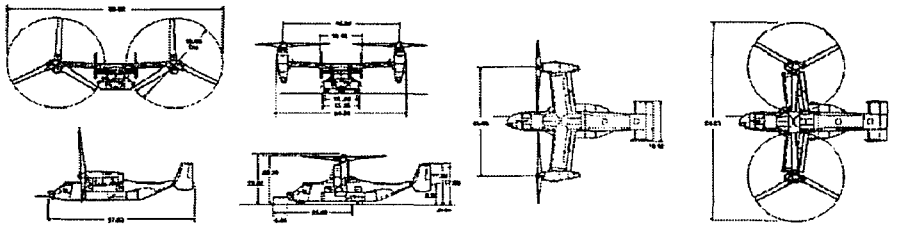

Figure 2: Schematic of the V-22 tiltprop [13]

Upper surface blowing, $\Lambda = U$, is a technique of jet based propulsion system that enables high lift at low speeds. As depicted in Figure 3, this configuration of the engine over the main wing causes the high velocity exhaust to generate very low pressure, thereby enhancing lift [8] and shortening the ground roll distance for takeoff. Vehicles with upper engine configuration are confined within mid to high subsonic speeds due the presence of engine nacelle as flow speed increases above the wing [15]. Hence, the cruise speed remains well below the supersonic regime. Type *U* configurations have been deployed on military, medium speed jet transports such as the An-72 in Figure 4.

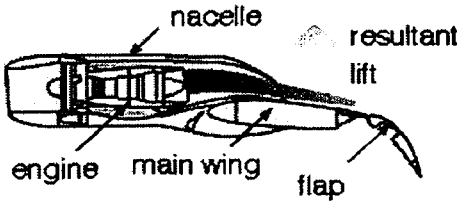

Figure 3: Upper engine schematic of Aska [13]

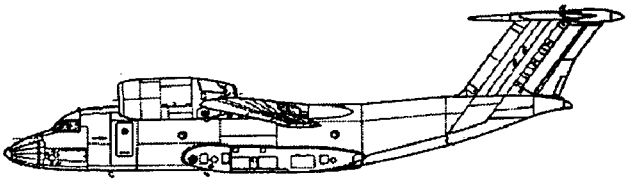

Figure 4: Upper engine configuration of An-72 [14]

Situation of engine units are normally below the wing for transport vehicles, where they do not require enhanced takeoff capabilities. Yet this conventional engine configuration, $\Lambda = C$, may be configured for V/STOL operations by the deflection of engine exhaust downwards via the main wing or flaps. Related studies have shown that interactions of engine exhaust and the main wing increases the effective lift coefficient as a function of the thrust

[8,16]. Type C configurations are found to be effective on the C-17 and other military transports. The drawback of this design is the deflection of flow that inevitably causes a reduction in effective thrust. Experimental results reveal that loss of thrust via type C engine deflection is relatively higher than type U configurations described previously [17,18].

Thrust may be used to enhance lift by the vectoring of nozzles. This is typically found on V/STOL capable aircrafts where the entire propulsion system is fully integrated into the main body; e.g. performance fighters. In early stages of research, it was strongly believed that the redundancy provided by multiple engine units is required for vertical takeoff in the case of an engine failure. The progressive increase in engine reliability has enabled V/STOL operation via a *single lift-cruise* engine unit for both lift and cruise thrust, $\Lambda = S$, reducing the weight of the deployment system and enhancing the overall mission effectiveness of the vehicle. The type S configuration supports V/STOL operations by balancing between the compressor thrust and turbine thrust about the vehicle's centre of gravity [19,20]. Careful arrangement of engine exhaust with respect to the main wing reduces the effects of suck down, and the force of rebounding air may be maximised. In corollary, cool compressor thrust is circulated to the induction system, eliminating the effect of hot air ingestion. In practice, a large bypass compressor flow is required to balance the thrust produced by the exhaust during vertical deployment. Thus, the frontal area of the AV-8 is apparently large to accommodate the engine installation. This has limited the vehicle's flight envelope within the subsonic regime. Shown in Figure 5 are the F119 engine of the X-32 and the Pegasus engine of the AV-8. The F119 core thrust nozzle pitches up to 20°. The resultant pitching moment is balanced with the compressor thrust during short takeoff operations.

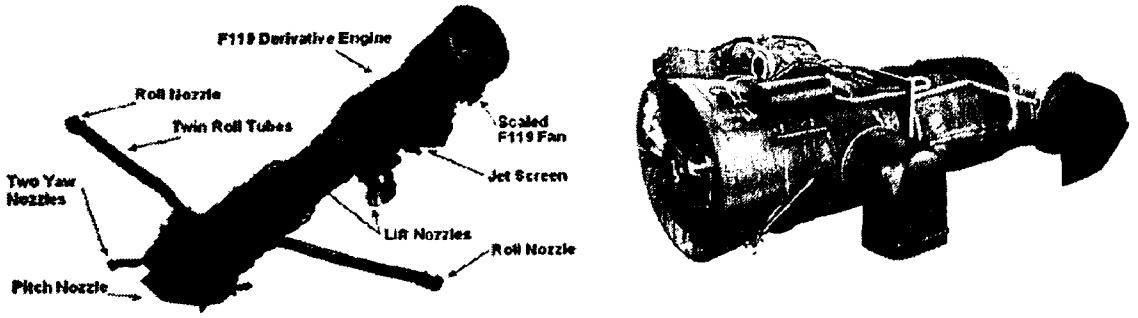

Figure 5: STOL X-32 [13], and VTOL AV-8 [21] deployment systems

Recalling the early stages of V/STOL research, developers at Yakovlev had realised that type S design may not satisfy both vertical takeoff and supersonic cruise requirements [10]. A *dual lift-cruise* deployment system, $\Lambda = D$, bridges two such design requirements by separating the propulsion department for takeoff and for cruise. This type D system permits

more design freedom in terms of airframe integration and the transfer of propulsive power. Figure 6 presents two production designs that utilise type *D* system configurations. Although the Yak-38 was successful at performing vertical deployment and supersonic flight, the unused weights of the lift engines during cruise have set back its operation range. It was also suspected that significant time was required to engage the lift engines [10]. The above concerns have been perceived in the development of the short takeoff F-35B. The multirole fighter utilises a 90° swivelling nozzle and a lift fan that is driven by the core engine through a gearbox, which is responsible for disengaging the lift fan during cruise. The lift component is therefore light weight and consume on engine load during other phases of flight.

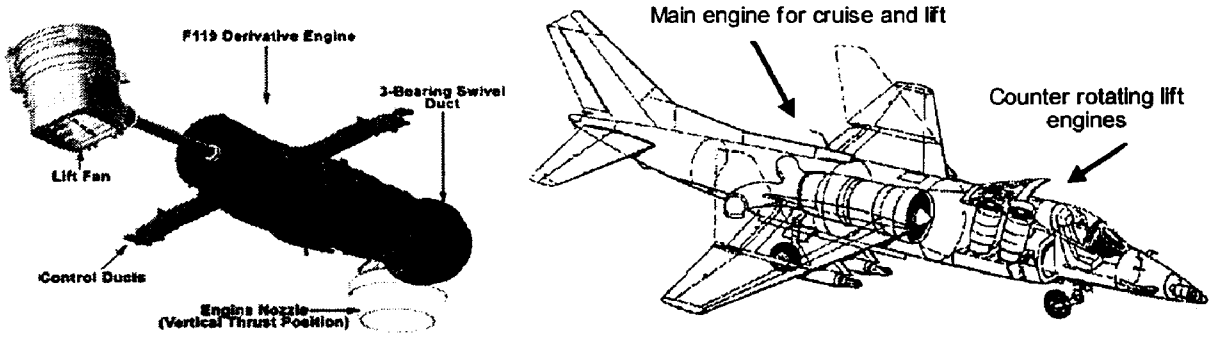

Figure 6: Deployment systems of the short takeoff F-35B [14] and the vertical takeoff Yak-38 [10]

3 EXPANDABLE ENGINEERING EXPERT SYSTEM: E³

3.1 Framework

E³ is constructed under the Matlab 6 [21] high level programming environment, in which the available engineering analysis and AI tools that are conveniently adapted. While E³ does not have a central governing program, its construction is based on infrastructures found in most expert systems [22]. The architectural compositions of E³ are presented as a schematic in Figure 7. Following the conventions of expert systems, the knowledge storage unit is separated from the knowledge control unit such that information may be modified and updated independently [22,23]. Respectively, they are known as the knowledge base and the inference engine in Figure 7.

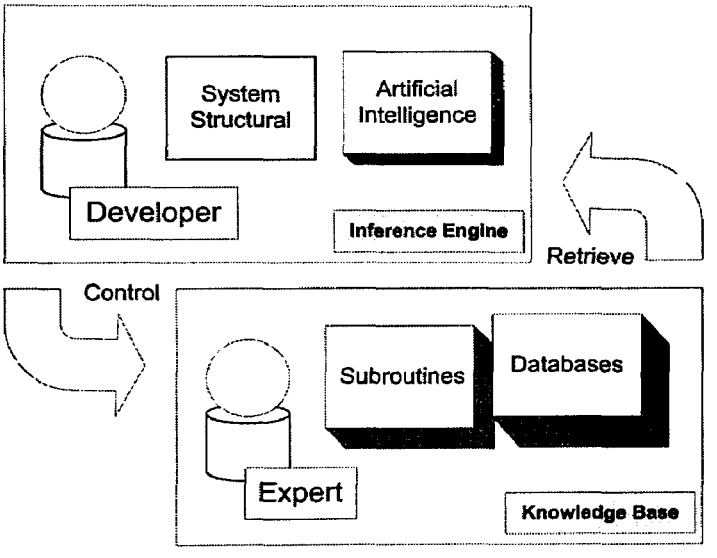

Figure 7: Expert system infrastructure, E³

The structural component establishes a systematic method of allocating of memory and files to the problems of interest. AI modules are constructed directly under the Matlab environment and are independent of the system structure. This enables E³ to adapt to other AI problem solving tools, and to be broadly applied to various problems. The database unit, in theory, constitutes the largest memory block of E³. It is summoned appropriately when statistical analyses are required. While Matlab supports various data formats such as text or spreadsheet files, individual subroutines are standardised in the form of Matlab functions. The standard format shown in Figure 8 identifies the files for indexing and documentation to communicate to the end user, and to the inference engine. The knowledge base subroutines

can be executed in solving a particular problem. A complete listing of files within E³ is found in section A.1.

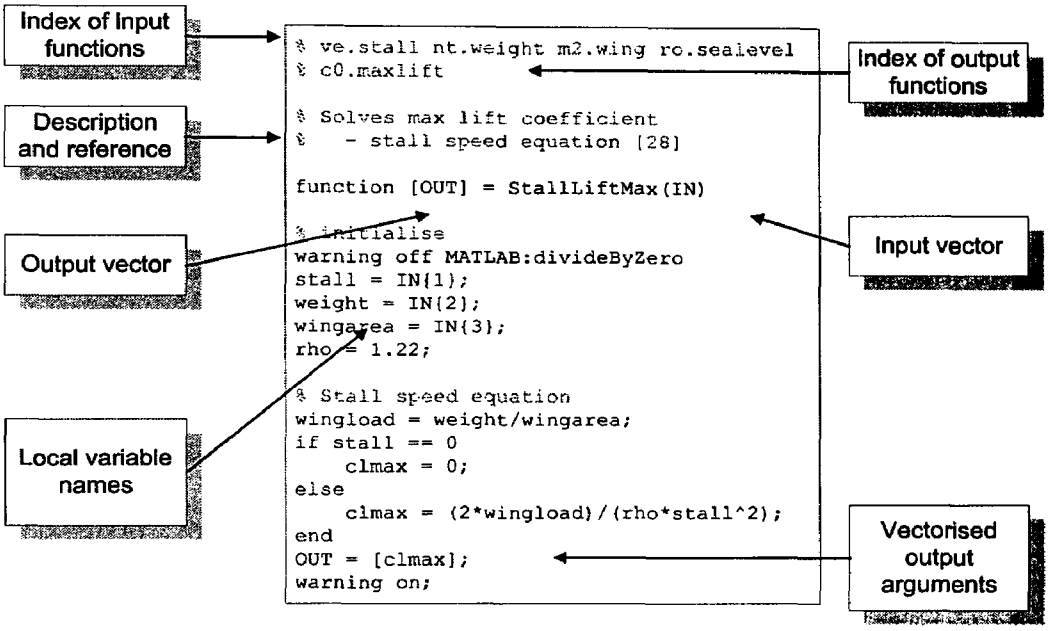

Figure 8: Example of a subroutine function

Variables that are used in the solution of a specific problem, or the working variables, reside in the Matlab structured variable called the *blackboard*. They are hieratically categorised further by different scientific quantities. Figure 9 is a sample variable of planform area S in Matlab coding; and Figure 10 is the schematic of the blackboard structured variable.

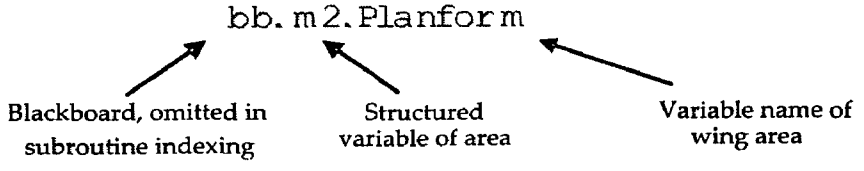

Figure 9: Sample working variable coded in Matlab

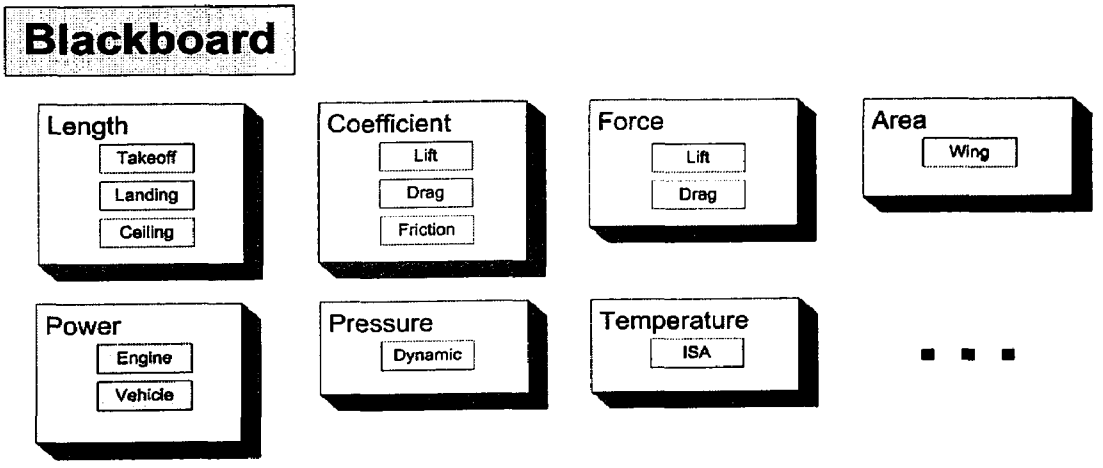

Figure 10: The structured variable of blackboard, and sample working variables

The general framework of E^3 provides a foundation for the cross referencing of subroutines and data, resulting in a network of knowledge.

3.2 *Parametric Problem Solving*

A problem solving alg orithm is developed to automate the execution of subroutines corresponding to the problem specified. As a component of AI, this parametric search module provides extensive support to the mathematical formulation of engineering problems. The search begins by uploading the known parameters and the unknown parameters as null entries to the blackboard memory, as indicated on the top of Figure 11. During the operation of the search, the validity of each subroutine of the knowledge base is evaluated by comparing the known and unknown parameters of the blackboard against the input and output of each subroutine indexed by the first two lines of Figure 8. The matching subroutine is then performed, solving for the unknown values. In cases where there are no exact matches found, the algorithm executes any solvable subroutine based only on the available input. The corresponding outputs are returned to the blackboard as additional resources for the next search recursion. This process is iterated until, or all unknown parameters are found or all solvable subroutines have been executed. In effect, a solution is determined through a search of the knowledge base.

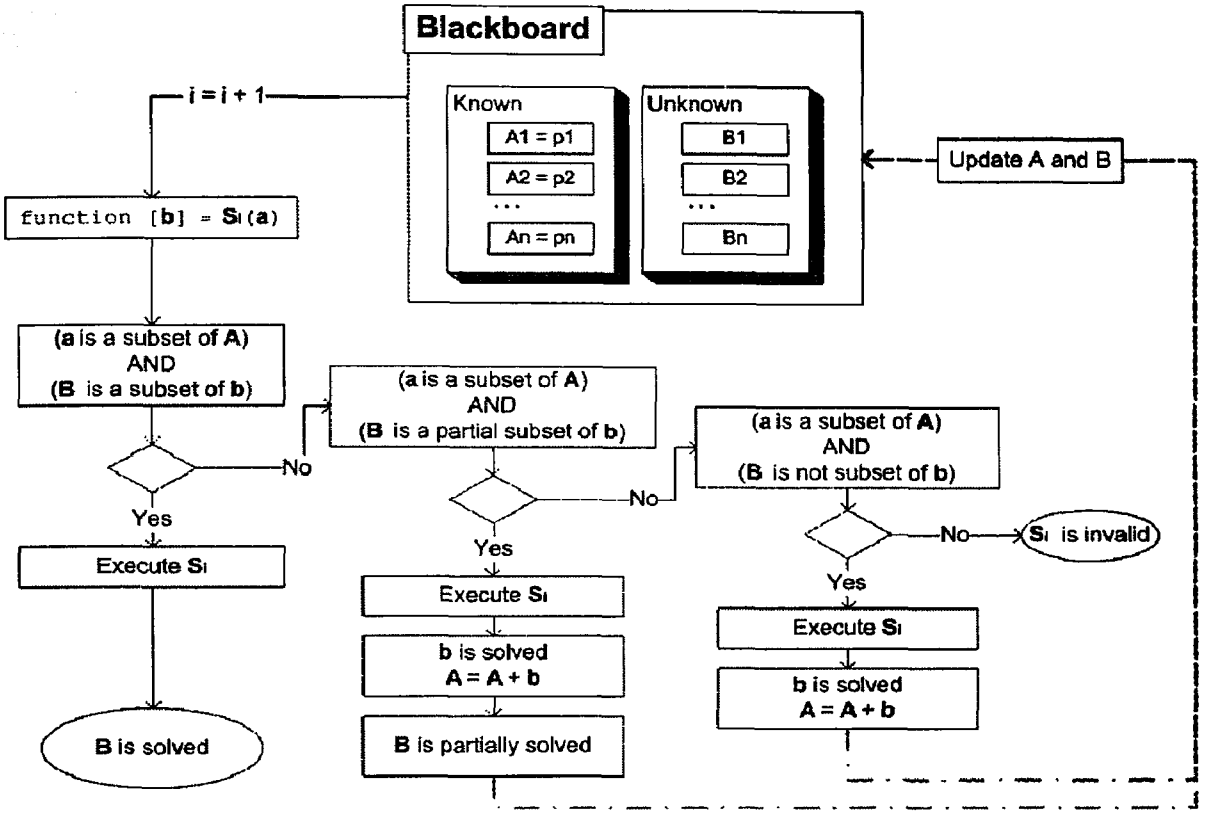

Figure 11: Flowchart of the parametric search algorithm

3.3 *Fuzzy Reasoning*

General AI systems are made up of decisive rules such as 'if a then b'. However, it is difficult for conventional logic to evaluate such a rule when a or b are expressed qualitatively. Here, fuzzy reasoning provides the means to evaluate qualitative values by first classifying numerical values. Figure 12 shows the takeoff distance, $X_{takeoff}$, fuzzified into three categories represented by three membership functions. The degree of membership δ, a scale between 0 and 1, determines the applicability of the categorical definition, or simply how well a membership describes a value.

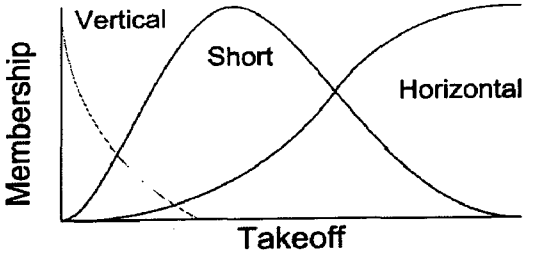

Figure 12: Three categories of takeoff lengths

In other words, a value of $X_{takeoff}$ may be represented by a vector as[a]:

$$\begin{bmatrix} vertical \\ short \\ horizontal \end{bmatrix} = \begin{bmatrix} \delta_1 \\ \delta_2 \\ \delta_3 \end{bmatrix} \quad (1)$$

Hence, rules that appear to be conflicting in discrete logic may now be simultaneously applied, such as:

```
'if takeoff is vertical...'

'if takeoff is short...'

'if takeoff is horizontal...'
```

The weight of each rule is fundamentally dependent on the degree of membership describing the terms. The influence of each rule may be aggregated through a number of methods, resulting in a fuzzy, or defuzzified output value. The development of D² utilises the Fuzzy Inference System interface provided by Matlab to deduce a qualitative description of the deployment configuration as part of the expert system's knowledge base.

3.4 Neural Network Regression

Airplane design often requires statistical data for preliminary analysis, wherein conventional curve fitting methods are often used. However, it may be difficult for convention curve fits to model complex behaviour of data presented. The concept of neural network was recognised to be a valuable tool in pattern recognition in the 1980s [23], e.g., in predicting unknown functions. Like a biological neuron, a single unit of an artificial neuron summates and evaluates inputs through an activation function. If activated, the neuron sends an output signal linking to other neurons or interprets the final output. The associated weight factor of each neuron changes to adapt to a specified output. This training process enables the learning capability for interconnected neurons, or a neural network.

Among various types, the generalised regression neural network is found to be most compliant in function approximations [24]. This is provided that the number of sample data for training is sufficient and are reasonably distributed over the domain to be modelled.

---

[a] The vector is unique provided that the membership functions do not share a single axis of symmetry along the measuring value.

Figure 13 contains a set of sample data, which exhibits both parabolic and logarithmic behaviours. Although a 4th degree polynomial curve fit can be implemented with relative ease with Matlab, the model fails to interpret the concavity of the data trend correctly. In contrast, the generalised regression networks are not constrained by the definite degrees of freedom of analytically derived curve fits and are able to follow the sample data at different levels of generalisation[a]. Furthermore, the use of neural network compromises a value on non unique data by weighting averages, e.g., the data that is marked x in Figure 13, whereas mathematical curve fits often encounter difficulties in this respect.

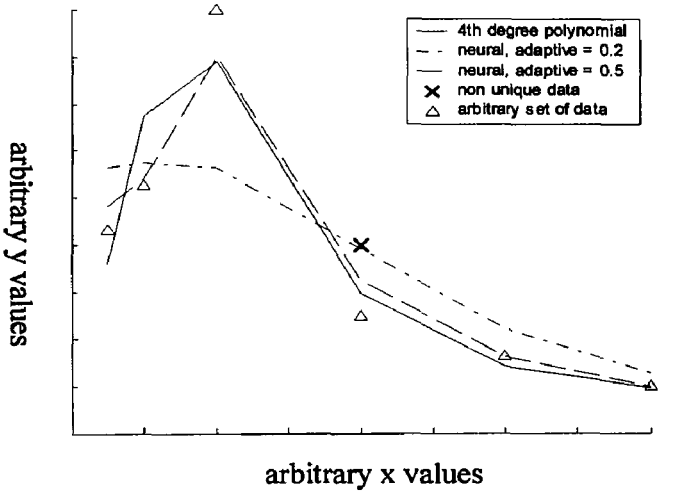

Figure 13: Comparisons of curve fits to an arbitrary set of data exhibiting both parabolic and logarithmic behaviours

In the interest of this study, series of sample data are fed into a neural network; and a scalar output is considered, corresponding to a multiple input single output system. The neural network adapts to each sample record of input $[a_1 \quad a_2 \quad a_3]$ by changing the weighing parameters to the target output x. A complete set of sample training data is represented in equation 2:

$$\left[\begin{array}{ccc|c} a_1 & b_1 & \cdots & x_1 \\ \vdots & \vdots & & \vdots \\ a_n & b_n & \cdots & x_n \end{array}\right] \tag{2}$$

A trained neural network may then approximate an output value x, given an arbitrary input vector $[a_1 \quad a_2 \quad a_3]$. Hence, a neural network may be seen as an approximation function as equation 3, only that it is dynamically referenced to a statistics of sample data.

---

[a] This is related to the formulation of the radial basis network, a sub network of the generalised neural regression model, which generates as many neurons as the number of training samples [21].

$$x = neural(a, b, ...) \tag{3}$$

In a generalised regression neural network, the response of the network to each sample data can be adjusted via an *adaptive* parameter[a]. This parameter governs the degree of influence on x by nearby sample data. Refer again to Figure 13; the smaller adaptive value corresponds closely to the actual data plots. As the parameter is increased, the network tends to generalise the system. However, this may not be absolutely desirable; and the network may not produce estimations over a wide domain.

Based on the generalised regression neural network algorithm of Matlab, E^3 provides an algorithm to automatically generate a network given a database of training samples. The algorithm also serves to scale the adaptive parameter, beginning from a small initial estimation. Then, should the network fail in producing an estimate, the adaptive value is increased to simulate a more general approximation. However, since the adjustment of the adaptive parameter must be proportional to the magnitude of the training values, it is often difficult to project how much the parameter must be increased. Here, E^3 regulates this by normalising the training data with respect to an average, such that the range of data can be condensed. This repetitive task of training and calibration of neural network requires a significant amount of computation resources that is proportional to the size of the training database[b].

3.5 Deployment Design Process

Constructed within the knowledge base, the deployment design subroutine D^2 derives a deployment system most suitable to the design requirements, by networking with AI, subroutines, and databases under the establishment of E^3. The process of D^2 is divided into five analysis phases, as described in Figure 14. The process is initiated by a user specified set of inputs and is converted to the standard performance parameters, known as the *primary inputs*:

$$W\ ,\ X_{takeoff}\ ,\ X_{landing}\ ,\ M\ ,\ Z \tag{4}$$

---

[a] This is also known as the measure of *spread* [21].

[b] The neural network module of E^3 also serves to approximate values that are missing in the training data by successive generation of neural networks. However, this is not recommended as estimation errors may easily propagate such that the accuracy of the network is reduced.

The maximum takeoff weight W is a fundamental design parameter as it appears through flight mechanics analyses. $X_{takeoff}$ and $X_{landing}$ are the takeoff and landing ground roll distance, respectively. Together they specify the deployment requirements. Secondly, the flight Mach number M and the cruise altitude Z, enable the vehicle's operation condition to be described. By fuzzifying the input requirements, a deployment-propulsion configuration is deduced. The analysis proceeds in determining the intermediate parameters by referring to the AI module and knowledge subroutines. The following parameters are the *design outputs*, which determine the configuration of the deployment system:

$$\Lambda\ ,\ \ T_{engine}\ ,\ n\ ,\ W_{engine}\ ,\ d\ ,\ \beta \tag{5}$$

Since the analysis of D^2 focuses on the thrust based propulsion systems, the parameters of unit thrust T_{engine} and the bypass ratio β together specify the output requirement of either turbofan or turbojet engines. Λ is a qualitative term describing the configuration type, i.e. the general layout of the deployment system. The number of units n, the engine unit weight W_{engine}, the engine bypass ratio[a] β and engine cross section diameter d are the engine specifications that further describe the deployment system. In addition, an optimum thrust vectoring angle for takeoff [6] may also be deduced. Each phase of the D^2 analysis shown in Figure 14 will be further discussed in section 4.

[a] Defined as the ratio between the cold air exhaust from the compressor and the hot combustion exhaust.

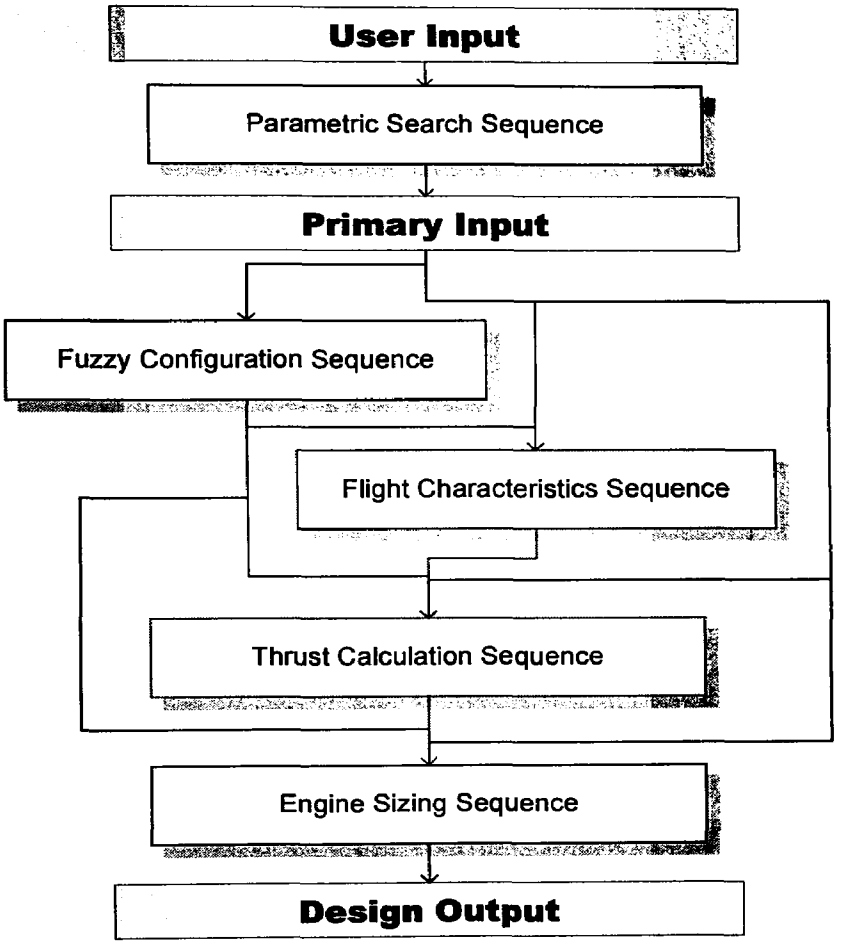

Figure 14: Expert system design process: D^2

4 PROCESS OF DEPLOYMENT DESIGN: D²

4.1 Parametric Search Sequence

Performance measures may differ from one vehicle type to another. To suit various forms of this design problem, the user specified set of inputs is converted to the primary input of 'equation' 4. This is facilitated by the execution of the parametric search module, a 'problem defining' sequence of D². The parametric module utilises the available values from the blackboard as the known variables. At the start of the execution of D², the only values available from the blackboard are the set of user input. The module resolves for the objective output by searching for the appropriate subroutine functions, which becomes the primary input parameters for the successive process sequence. This standardisation to the primary inputs ensures that the design is solvable, and the result of D² is conclusive prior to engaging in extensive computation. Figure 15 demonstrates the solution path based on a set of arbitrary input parameters. The empty weight[a] W_{empty} is used to obtain $W_{takeoff}$, or simply W. A common practice is the use of linear interpolation [7], as found in appendix A.2, and is represented by the subroutine *EmptyMaxWeight*. The primary input of Mach number M is deduced through the subroutines *AltitudeCondition* and *SpeedMach* from a user specified speed, v.

[a] According to the conventions of the vehicle design [26], W_{engine} is often approximated from the requirement of payload capacity.

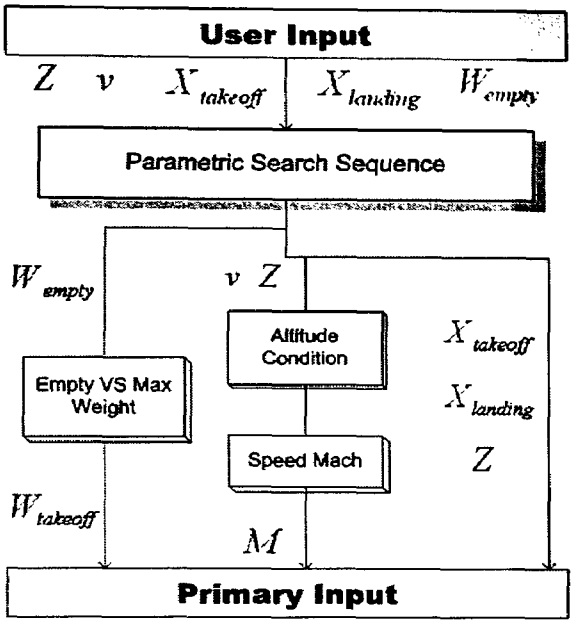

Figure 15: Sample solution path of the search module

4.2 Fuzzy Propulsion Configuration Sequence

Engineering design problems may be described as the balance between performance and economy. Following this philosophy, the deployment configurations discussed in section 2 are classified according to their relative measures of propulsive efficiencies, here on an arbitrary scale. The configuration types are abbreviated as the following types: H, P, U, C, S, D. Depending on the mission requirements, a design may shift on the scale of Figure 16. Note this empirical design approach is used only to correlate the configurations types, such that expert rules may be applied.

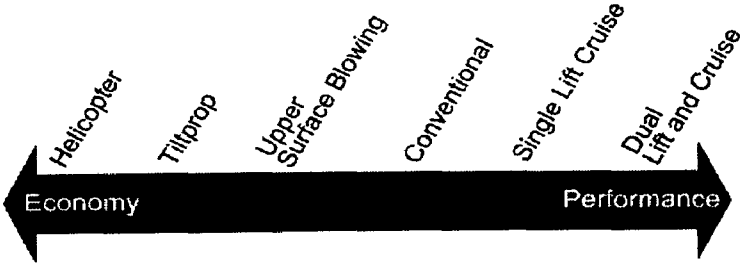

Figure 16: Evaluation of propulsion configurations in terms of propulsive efficiency

Based on the fuzzy logics presented in section 3.3, the above scale is adapted to a fuzzy model of determining one of the above types. First, the following inputs are fuzzified by the respective membership functions as follow:

- $W \rightarrow$ Light, Medium, Heavy
- $M \rightarrow$ Low subsonic, High subsonic, Transonic, Supersonic

- $X_{takeoff}$ → Vertical, Short, Horizontal
- $X_{landing}$ → Vertical, Short, Horizontal

The names of membership functions above are labelled according to the related aeronautical terms, in which they qualitatively describe the conceptual design. For example, the fuzzy module may interpret the Boeing 747 as a heavy, transonic vehicle that takeoff and land conventionally, in other words, horizontally. Next, the general design and specialised V/STOL knowledge are translated into fuzzy rules. Some are:

```
if (Takeoff not Vertical) and (Landing not Vertical) … then (Type is S)

  if (Takeoff is Vertical) and (Mach is LowSubsonic) then (Type is P)

                              ⋮
```

Next, all fuzzy rules are aggregated, resulting in an output value of configuration. Since the scale of 'configuration' is based on an arbitrary scale from Figure 16 and does not represent a meaningful quantity, an additional refuzzification subroutine determines the configuration type $\Lambda_{selected}$ that most describes the output quantity, along with its degree of membership $\delta_{selected}$, and the next viable configuration $\Lambda_{alternative}$ based on the next highest membership. For example, an input of primary inputs that resembles a regional aircraft results in an arbitrary 'configuration value' that is described by the membership function P for tiltprop at a degree of 0.6, and below 0.6 by the function C. The values are thus $\Lambda_{selected} = P$, $\delta_{selected} = 0.6$, and $\Lambda_{alternative} = C$, respectively. The complete sequence of fuzzy analysis is outlined in Figure 17.

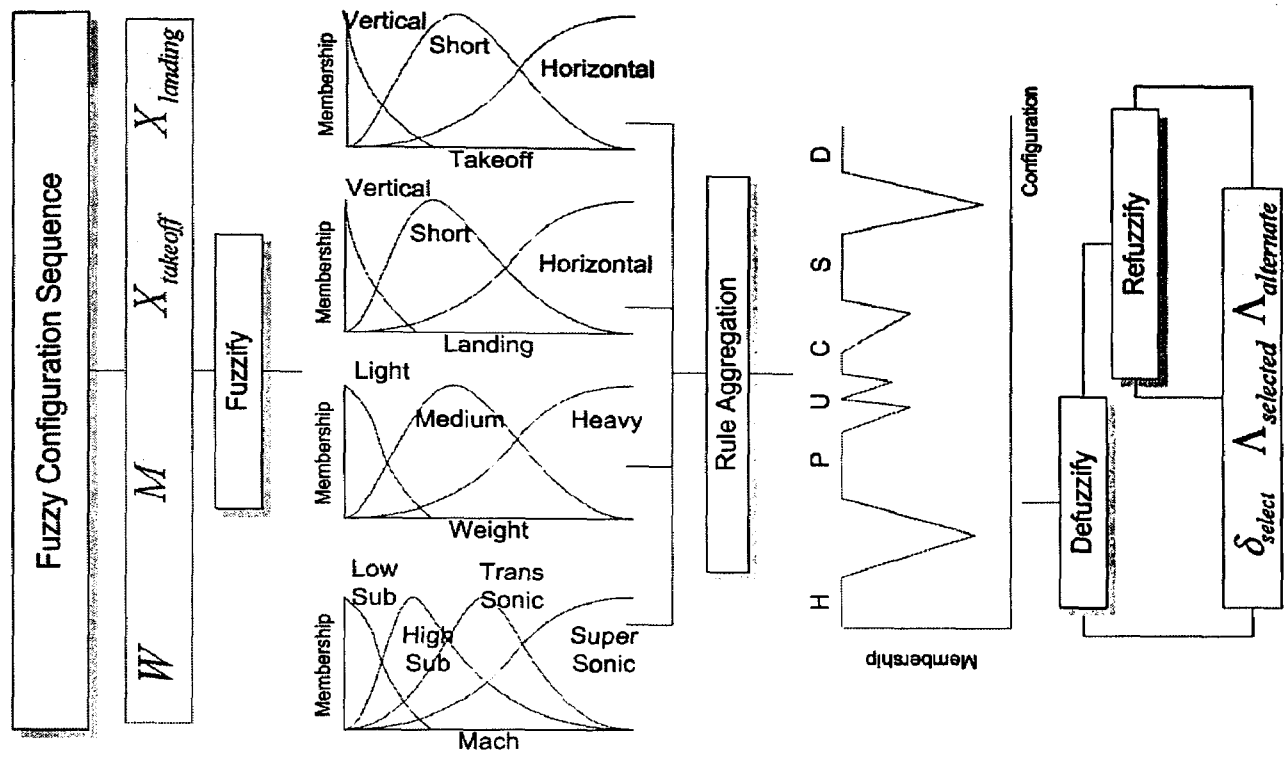

Figure 17: Flowchart of fuzzy reasoning

In this study, the parameters of the input and output membership functions are empirically determined such that the fuzzy system accurately portrays the configurations of existing airframe designs found in appendix A.3.1. The configured fuzzy system may be functionally written as:

$$[\Lambda_{selected}, \delta_{selected}, \Lambda_{alternate}] = fuzzy(W, M, X_{takeoff}, X_{landing}) \quad (6)$$

4.3 Flight Characteristics Sequence

The estimations of basic flight characteristics are necessary in the support of performance analysis. This module hypothesises the aerodynamics properties regarding the vehicle of interest. Related statistical data are queried from A.3. From this point on, analysis refers only to thrust based propulsion systems of type *U, C, S, D*.

The aspect ratio σ and the planform area S of a vehicle's main wing are estimated via the generalised regression neural network. It is found that the input parameters associated with equations 7 and 8 portray equations of flight and statistical data most accurately. The input parameter M is included in equation 7, to describe the behaviour of σ in two flight regimes. First, high σ is typically found on subsonic vehicles, due to the beneficiary of flight efficiency of the wing [26]. However, at transonic or supersonic speeds, potential shock losses restrict σ to be lower. On the other hand, the wing area S is heavily dependent on the

vehicle's size, described by W. The parameter wing loading W/S determines the performance of takeoff and the achievable cruise speed.

$$\sigma = neural(W, M, Z, X_{takeoff}) \quad (7)$$

$$S = neural(W, M, X_{takeoff}) \quad (8)$$

Sample data for the training of the above neural networks suppose that, for vehicles of type H:

$$\sigma = S = 0 \quad (9)$$

Although the above definition enables neural networks to model non wing designs, it may negatively affect estimations of fixed wing aircraft with vertical takeoff capabilities to some extent.

Estimation of the maximum lift coefficient is accomplished through the following relationship derived from an equilibrium modeling of steady flight [26]:

$$\hat{c}_L = \frac{W}{0.5\rho S v_{stall}^2} \quad (10)$$

The stall speed v_{stall} is found from the neural network approximation of equation 11[a]. The inputs of the neural network are selected based on the relationship between the weight, the flight speed and the takeoff performance of aircraft.

$$v_{stall} = neural(W, M, X_{takeoff}) \quad (11)$$

$\hat{c}_L$ is obtained via substitution of equation 11 into equation 10. This value is assumed as the maximum lift at an approach configuration. For the calculation of takeoff kinematics, the following relation is supposed:

$$\hat{c}_{L,takeoff} \propto \hat{c}_{L,approach} \quad (12)$$

Proportionality constants are added to the above relationship based on the statistical findings of different vehicle types [7], and the verification of takeoff calculations, as in Figure 18.

[a] A comparison of equation 11 with other neural network models can be found in A.3.

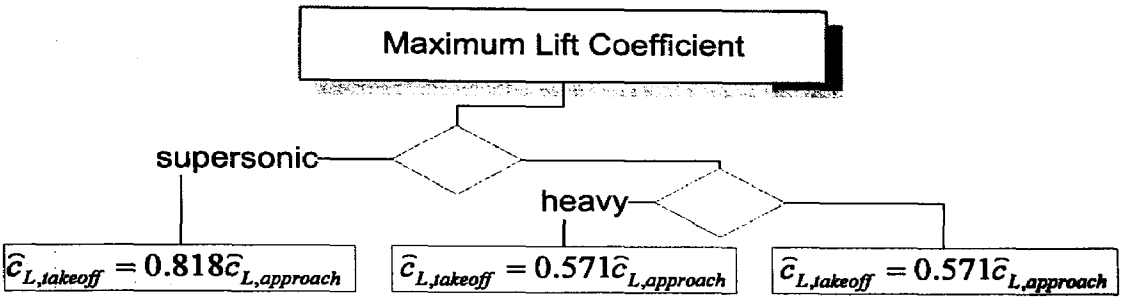

Figure 18: Fuzzy classification of maximum takeoff lift coefficient

Significant amounts of thrust on aerial vehicles are used to overcome drag. However, it is difficult to evaluate vehicles' drag at the conceptual design phase precisely, since this requires the geometry of the vehicle to be clearly defined. This study introduces equation 13 as coarse estimates of minimum drag $\breve{c}_D$ [a] [7,26]:

$$\begin{aligned} \breve{c}_{D,takeoff} &= \breve{c}_{D,landing} = 0.100 \\ \breve{c}_{D,cruise} &= 0.020 \end{aligned} \tag{13}$$

4.4 Thrust Calculation Sequence

The design output parameters describing the propulsion system must satisfy all of the following deployment requirements, along with the cruise conditions criteria. This is defined by the primary input parameters:

- Liftoff before $X_{takeoff}$ is reached.
- Cruise at a specified M.
- Climb to the service ceiling of Z.
- Complete landing rollout within a distance of $X_{landing}$.

Equation 14 represents the gross thrust value.

$$T_{required} = \max\left(T_{takeoff}, T_{Cruise}, T_{Altitude}, T_{landing}\right) \tag{14}$$

Figure 19 is a flowchart for determining $T_{required}$ within D², in which decisions are based on discrete and fuzzy input parameters. For example, the subroutine '*Mach Thrust*' serves to find the thrust required to achieve the specified flight speed based on subsonic drag modeling. Therefore, the configuration type must be thrust rated and at a subsonic speed indicated by $M < 0.9$.

[a] Drag at zero angle of attack.

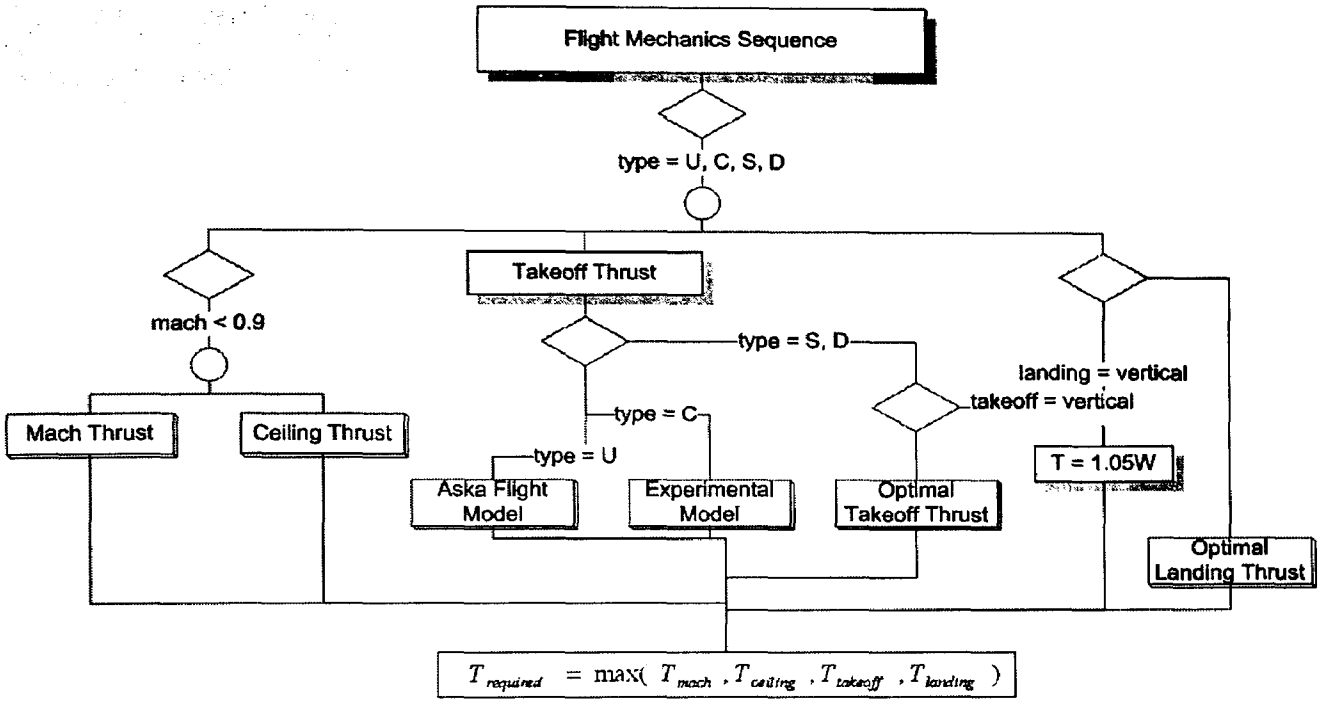

Figure 19: Flowchart of gross thrust requirement

The analysis of takeoff is described in Figure 20, and equations of motions are expressed in acceleration terms as equation 15 [6]. The forces included are lift, drag, weight, ground friction and thrust that is measured at a pitch angle τ.

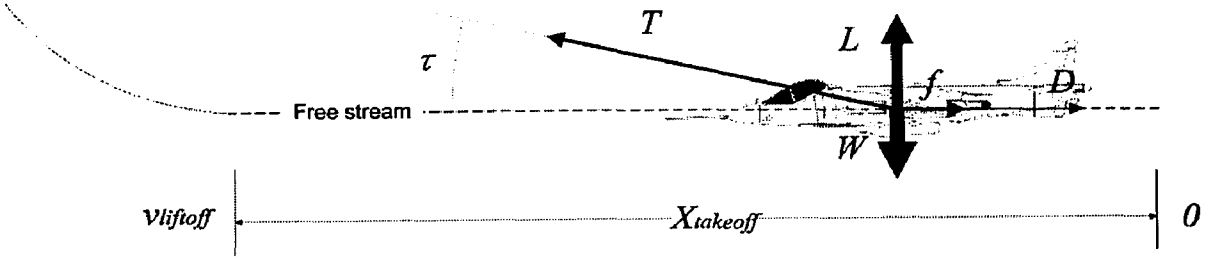

Figure 20: Forces at takeoff [6]

$$a_z = \frac{W - L - T\sin(\tau)}{m} \qquad a_x = \frac{T\cos(\tau) - D - \mu(ma_z)}{m} \qquad v = \int a_x dt \qquad x = \int v dt \qquad (15)$$

A time series simulation model of equation 15 solves for the thrust required, according to the specified takeoff run requirement:

$$x \le X_{takeoff} \qquad (16)$$

An indication of equation 15 is the presence of an optimal thrust vector angle, for which takeoff can be achieved at the minimal thrust needed. Equation 17[a] is a numerical solution for the optimal thrust vector under the takeoff criterion specified by equation 18.

$$\overline{T}_{takeoff} = numerical\left(W, X_{takeoff}, v_{stall}, \breve{c}_D, S, Z\right) \tag{17}$$

$$L_{rotation} + T\sin(\tau) \geq W \tag{18}$$

Equations 17 and 18 are implemented into subroutine function *TakeoffThrustVector*. Figure 21[b] is a sample calculation of an optimum thrust angle for the Sea Harrier from the inputs provided by A.3.1.

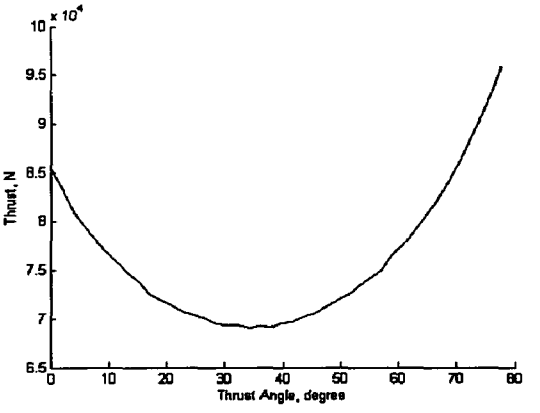

Figure 21: Takeoff thrust vectors of the Sea Harrier

Equation 19[c] is used to approximate the required thrust for vertical takeoff vehicles, with an excess of 10% thrust to account for losses, engine bleed stability control and upward acceleration.

$$\begin{aligned} T &= 1.10 \times W \\ \tau &= 90^\circ \end{aligned} \tag{19}$$

---

[a] Alternatively, equation 15 can be expressed in the form of a nonlinear differential equation, where the boundary conditions are given by the initial and final takeoff displacements. An optimal thrust vector can be found at each increment of time, thereby producing an optimal takeoff trajectory of thrust pitch. Full solution is not presented here due to the extensiveness of the final expression.

[b] Note the local areas of instabilities, i.e., jittering of the curve, due to the step size of numerical integration. This must be suppressed in actual simulation. Here, it does not obstruct the purpose of this demonstration.

[c] More appropriately, the takeoff thrust for V/STOL vehicles should include an excess thrust needed for reaction control

As discussed in section 2, type *U* and C engine systems achieve V/STOL via the change of flow fields above and below the main wing, respectively, for an increase of lift. The increase in lift can be stated as a function of thrust [16]:

$$\Delta\bar{c}_L \propto c_T = \frac{T}{0.5\rho v^2 S} \tag{20}$$

The increase of lift resulting from equation 20 indicates that the takeoff criterion of equation 18 may be achieved sooner, thereby reducing the thrust required of each takeoff simulation. The effects of upper surface blowing and the deflection of engine thrust below the wing are strongly dependent on the arrangement between the engines and the main wing. Section A.5 attempts to model various *U* and *C* type designs via experimental and flight test results found in related researches [16,27].

The required cruise thrust is obtained via a subsonic drag model at flight equilibrium [26], where the wing efficiency parameter is omitted for simplicity:

$$T = D = 0.5\rho v_{cruise}^2 S\bar{c}_D + \frac{2\frac{1}{\pi\sigma}W^2}{\rho v_{cruise}^2 S} \tag{21}$$

The resultant thrust is rated at an altitude corresponding to the air density. Equation 22 translates the measure of thrust to a sea level condition via a density ratio [26].

$$\frac{T_{sealevel}}{T|_z} = \frac{\rho_{sealevel}}{\rho|_z} \tag{22}$$

$$T_{cruise} = T_{sealevel} \tag{23}$$

The thrust required to attain a specified service may be derived from a rate of climb of:

$$v_z = v\left[\frac{T}{W} - \frac{0.5\rho v^2 S}{W}\bar{c}_D - \frac{\frac{1}{\pi\sigma}W}{0.5\rho v^2 S}\right] \tag{24}$$

At the service ceiling, the reference rate of climb is $0.509 m/s$ [26]. Hence,

$$T_{altitude} = \frac{0.509}{v}W + 0.5\rho v^2 S\bar{c}_D + \frac{\frac{1}{\pi\sigma}W^2}{0.5\rho v^2 S} \tag{25}$$

The analysis of landing follows the dynamics described in Figure 22:

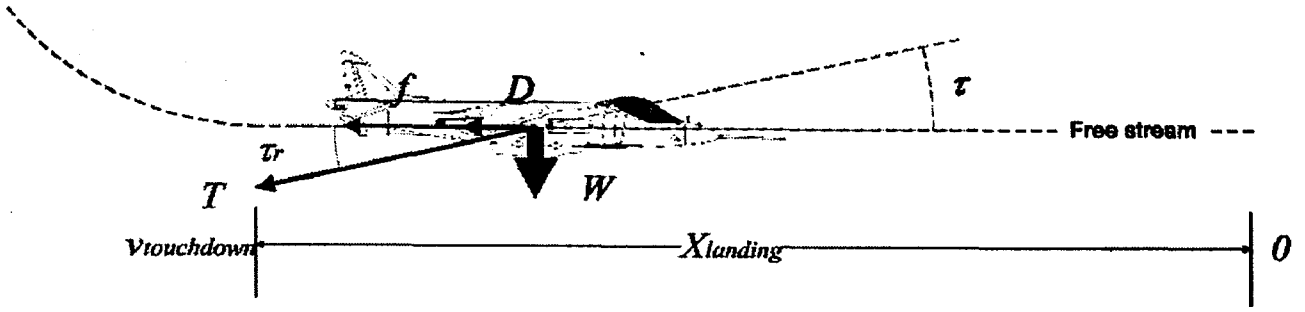

Figure 22: Forces at landing

It is found that the optimal angle that yields the minimum use of thrust can be approximated by the ground roll friction:

$$\tan \tau_r = \mu \tag{26}$$

The simulation of landing is analogous to takeoff, where $\tau_r = 180 + \tau$ and $W_{landing} = 0.6W$:

$$T_{landing} = |T_r| = numerical\left(W_{landing}, X_{landing}, v_{stall}, \hat{c}_{D,landing}, S, \sigma, \tau_r\right) \tag{27}$$

Although an important factor, thrust reversal losses are not included in the analysis of equation 27. For vertical landing vehicles determined by fuzzy categorisation, a direct force balance is used. To include a 5% loss or engine bleed control, landing is simplified to equation 28:

$$\begin{aligned} T_{landing} &= 1.05 \times W_{landing} \\ \tau_r &= -90^\circ \end{aligned} \tag{28}$$

4.5 Engine Sizing Sequence

The sizing of engines is derived from the overall thrust requirement of the vehicle and is characterised by the following specifications:

- Number of engine units
- Unit static thrust
- Unit dry weight
- Largest cross sectional diameter
- Engine bypass ratio
- Optimal thrust pitch angle

The final design outputs are deduced following the sequence of subroutines described in Figure 23.

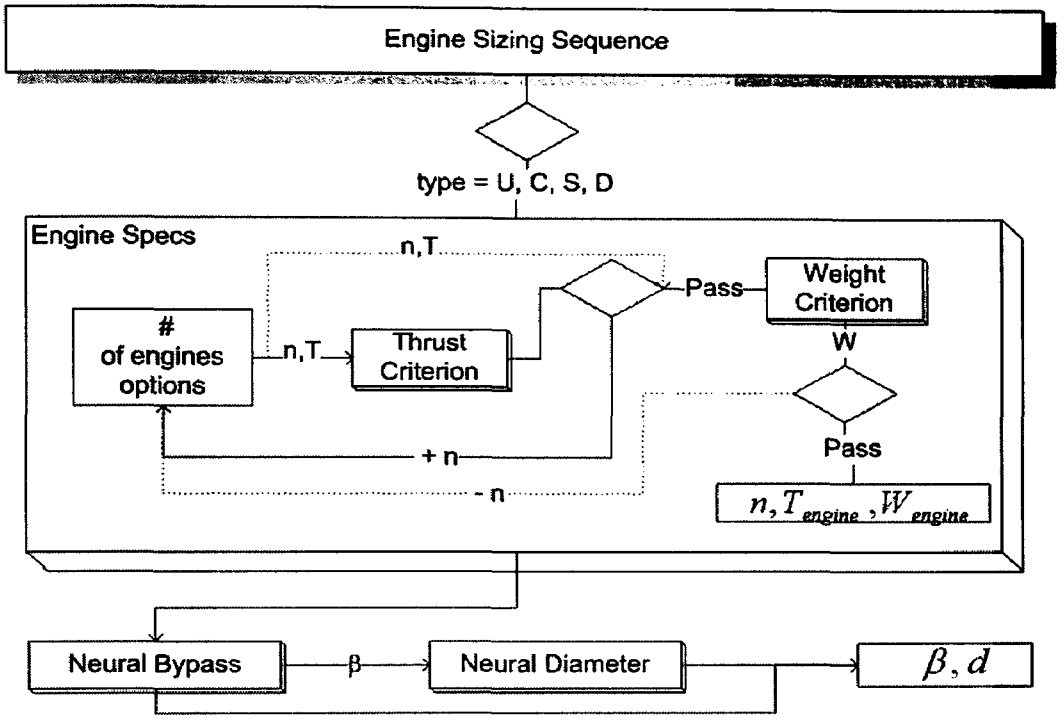

Figure 23: Flowchart of engine sizing sequence

The gross thrust requirement from equation 14 is fed to the engine sizing sequence to deduce the thrust output required by each engine units. The inclusion of an engine installation loss factor of 10%[a] results in $T_{equipped}$, the static sea level rating of thrust on the vehicle. This is written as equation 29.

$$T_{equipped} = \frac{1}{1.10} nT_{engine} = T_{required} \tag{29}$$

The unit weight of an engine is found to be proportional to the engine thrust [7]. This linear relationship is evident in Figure 24, where T_{engine} is plotted against W_{engine} based on A.3.2. Equation 30 describes such relationship and is used to deduce engine's dry weight.

[a] This factor varies, and may be as low as 6-7% [20].

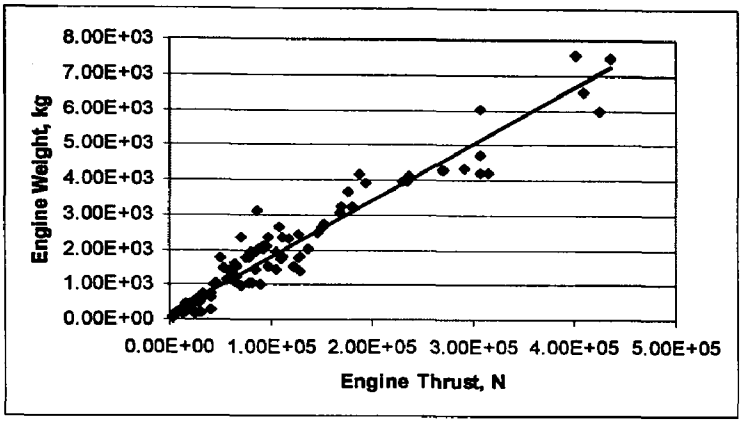

Figure 24: Engine weight versus engine thrust

$$W_{engine} = 0.0162T_{engine} + 171.5 \quad (30)$$

The combined weight of engines is maintained within a value referenced to a statistical trend of general airplane designs. This is done by referencing to the ratio between the weight of the propulsion system and the gross vehicle weight. Figure 25 is composed of a set of queried data from section A.3.1 and A.3.2.

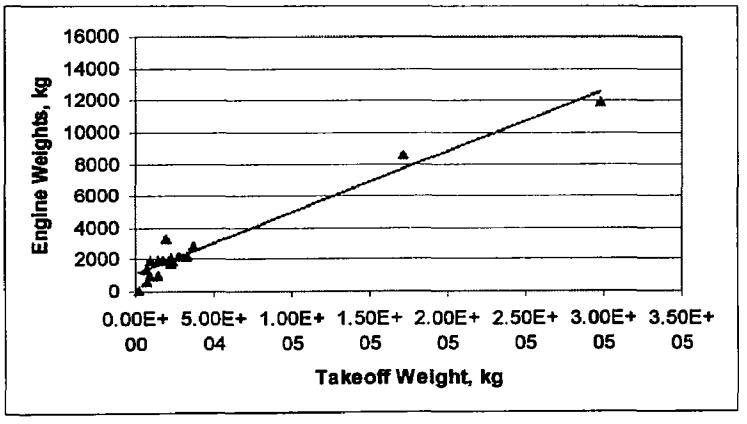

Figure 25: Weight ratio

$$W_{propulsion} = nW_{engine} = 0.0384W_{vehicle} + 1144.4 \quad (31)$$

The weight criterion function of equation 31 is a reference limit for $n \times W_{engine}$ in which a design should not exceed, based on equations 29 through 31. In practice, this line may be referenced higher or lower depending on the type of machine to design for. For example, V/STOL or military vehicles' weight ratios may reside in the region above the reference line to allow for larger propulsion systems. Since the addition of n only increases $W_{propulsion}$. The flowchart of Figure 23 indicates that the engine sizing module overrides the thrust criterion, which determines the upper limit of thrust output based on the database of appendix A.3.2, to satisfy the weight requirement.

The bypass ratio β and the cross sectional diameter are two influential parameters describing a vehicle's flight envelope and the relative airframe size for the integration of propulsion system. β may be used in further design developments for the determination of other propulsion properties including the geometry, maximum engine temperature, etc. To further describe the deployment system, D² facilitates estimation of both β and d via neural networks. In addition to W and T_{engine}, the approximation of β accounts M, based on the fact that β is generally large for heavier subsonic vehicles. And at supersonic speeds, β is very small to reflect the performance of turbojet engines. Meanwhile, d is a neural function of T_{engine} and the amount of cold air bypass, i.e. β. This is shown in equation 33[a].

$$\beta = neural(W, M, T_{engine}) \quad (32)$$

$$d = neural(T_{engine}, \beta) \quad (33)$$

[a] In actual design practice, the determination of β and d are influenced by the size of the airframe.

5 RESULTS

5.1 Fuzzy Module

The membership functions and the governing rules of the fuzzy inference module discussed in section 4.2 are determined to reflect actual airframe designs. This fuzzy system is found to be 90% in accordance with the deployment configurations of airframes found in A.3.1. Since the fuzzy model accounts for merely four input variables, it cannot achieve full accuracy due to exclusion of other design factors that have definite impact on propulsion settings, e.g., flight agility. Table 1 presents full comparisons of actual designs against the fuzzy results in shaded areas, including the fuzzified input values, the selected configuration type, its degree of membership, and the next viable configuration option following the flowchart of fuzzy reasoning in Figure 17. It is realised that the fuzzy definitions of $X_{takeoff}$ and $X_{landing}$ may be better interpreted on unit mass bases to portray vehicles of different sizes. Results of $\Lambda_{selected}$ are congruent to actual designs with relatively high confidence levels of certainty, as indicated by $\delta_{selected}$. Note for the Ka-22, the fuzzy system proposes a helicopter configuration, whereas the actual Ka-22 is a tiltprop design. This reflects the incapability of the fuzzy system to determine the configurations without the input of the service altitude, which differentiates the type *H* and type *P* designs.

Airframe	m	M	$X_{takeoff}$	$X_{landing}$	$\Lambda_{selected}$	$\delta_{selected}$	$\Lambda_{alternate}$
Sea Harrier	1.2E+04	1.25	305	0	Single	--	--
	Light	Supersonic	Short	Vertical	Single	0.56	Dual
JH-7	2.8E+04	1.70	920	1050	Single	--	--
	Med	Supersonic	Short	Horizonta	Single	0.61	Dual
Q400	2.9E+04	0.58	1014	1094	Tiltprop	--	--
	Med	HighSub	Short	Horizonta	Tiltprop	0.63	Upper
A400M	1.2E+05	0.72	1402	625	Tiltprop	--	--
	Heavy	HighSub	Horizontal	Horizonta	Tiltprop	0.65	Upper
YC-14	7.7E+04	0.60	572	610	Upper	--	--
	Med	HighSub	Short	Short	Upper	0.76	Tiltprop
Harrier AV-8B	9.3E+03	0.98	0	0	Single	--	--
	Light	Supersonic	Vertical	Vertical	Single	0.80	Dual
C-130J	7.0E+04	0.59	930	427	Tiltprop	--	--
	Med	HighSub	Short	Short	Tiltprop	0.80	Helicopter
Falcon 900	2.2E+04	0.87	1590	724	Conventional	--	--
	Med	Transonic	Horizontal	Horizonta	Single	0.85	Convention
VJ-101C	6.6E+03	1.30	0	0	Dual	--	
	Light	Supersonic	Vertical	Vertical	Dual	0.86	Single
An-72	2.8E+04	0.56	620	420	Upper	--	
	Med	HighSub	Short	Short	Upper	0.89	Convention
Ka-22	9.4E+04	0.29	0	0	Tiltprop	--	--
	Med	HighSub	Vertical	Vertical	Helicopter	0.89	Tiltprop

Table 1: Results of the fuzzy selection module

5.2 Neural Module

Results of the neural network regression closely portray actual values of conventional designs. However, since the amount of training data describing unconventional designs is relatively small, particularly for V/STOL vehicles, the ability of neural networks to recognise such designs is consequently less proficient. This problem may be solved by first filtering the training data for only V/STOL vehicles. Yet this sacrifices the accuracy of neural estimation due to the limited number of filtered data. Here, neural networks are trained by a set of thirty to fifty sample airplane data queried from the database of airframes A.3.1. The influence of neural estimations errors on latter flight mechanics calculation can be seen on Figure 26 and Figure 27 in section 5.3. Outputs of D^2 are emphasised in grey within each table.

Table 2 shows the neural estimation of aspect ratio. It is evident that estimation of V/STOL vehicles, such as the An-72 and the C-17A, is less precise, due to the scarcity of relevant data for training. The result for the Su-30 is also significantly underestimated, which is suspected to be caused by the lack of training data at high Mach regime. It was also found that σ also varies considerably with respect to the agility of supersonic military vehicles. Hence, the adaptive parameter of M is configured higher to somewhat maintain the network's generalisation.

Airframe	m	M	Z	$X_{takeoff}$	σ		ε
					Actual	Neural	
RJ70	4.31E+04	0.73	10670	983	9.00	9.93	10.4%
AH-1W	6.69E+03	0.23	4270	0	0.00	0.55	0.0%
737-900	7.90E+04	0.82	12500	2439	9.40	9.60	2.1%
767-200ER	1.56E+05	0.80	11550	2071	8.00	7.75	3.1%
CRJ200	2.15E+04	0.74	12500	1527	8.90	8.15	8.4%
An-72	3.30E+04	0.65	10100	620	10.30	7.69	25.3%
C-17A	2.65E+05	0.77	13715	2124	7.20	9.84	36.6%
Su-30	3.30E+04	2.35	17500	550	3.50	2.45	30.0%

Table 2: Sample results of aspect ratio neural approximation

Table 3 is a list of the neural estimation results of wing area S, as defined by equation 8. Note that the first three entries are for the helicopter configuration, referenced to the modeling of equation 9. The planform area of the RJ85 is portrayed with no error, based on the similar specifications of the RJ100 within the training data. The value of the V/STOL An-74 is significantly underestimated, again based on the limited V/STOL training data.

Airframe	m	M	$X_{takeoff}$	S		ε
				Actual	Neural	
R-MAX	8.80E+01	0.02	0.0	0.0	0.00	0%
23F	8.80E+00	0.05	0.0	0.0	0.00	0%
Ka-50	1.08E+04	0.26	0.0	0.0	0.00	0%
RJ85	4.40E+04	0.73	1043.1	77.29	77.29	0%
STOL CH801	9.75E+02	0.15	119.0	15.5	15.30	1%
GR. Mk 7	8.70E+03	0.98	0.0	21.37	20.25	6%
Rafale	2.45E+04	1.80	600	45.7	42.20	8%
A340-200	2.75E+05	0.86	3017	361.6	427.80	15%
MiG AT	7.80E+03	0.80	540	17.67	21.00	16%
An-74	3.65E+04	0.65	930	98.53	77.29	27%

Table 3: Sample results of wing area neural approximation

The quotation of stall speed differs among vehicle types and conditions such as flaps and the weight that is constant changing throughout flight. Sometimes, v_{stall} may only be estimated via the landing or approach speed. For this reason, assumptions were made in constructing the general airframe database in A.3.1. This is believed to be the primary source of error inherited by the neural estimation of equation 11 from the training data. Since this directly influences the estimation of $\tilde{c}_{L,takeoff}$, the calculation of takeoff thrust is affected consequently. Numerical thrust analysis from equation 17 shows a 10% variation of the v_{stall} may affect $T_{takeoff}$ by 8-17%. Result of the neural system is shown in Table 4. The stall speed of the Sea Harrier is somewhat underestimated, measured relative to other military vehicles of the same size, potentially due to the low indication of $X_{takeoff}$. Due to the overall margin of error, it is recommended that the v_{stall} obtained here should first be verified with other similar designs, as this significantly impacts on the accuracy of $T_{takeoff}$ calculation.

Airframe	m	M	$X_{takeoff}$	v_{stall}		ε
				Actual	Neural	
RAH-66	7.90E+03	0.26	0	0.0	0.0	0.0%
Yak-38	1.03E+04	0.96	0	0.0	0.0	0.0%
GR. Mk 7	8.70E+03	0.98	0	0.0	0.0	0.0%
RJ100	4.60E+04	0.73	1184	48.9	47.8	2.3%
MiG-31	4.62E+04	2.83	1200	72.5	77.7	6.6%
767-200ER	1.56E+05	0.80	2071	63.4	63.0	0.7%
Sea Harrier	1.19E+04	1.25	305	---	45.8	---
777-200ER	2.98E+05	0.84	3030	65.1	68.4	4.9%
CRJ200	2.15E+04	0.74	1527	69.4	54.4	27.6%
737-900	7.90E+04	0.82	2439	72.5	56.5	28.4%
IL-214	5.50E+04	0.75	1160	69.4	48.9	42.0%

Table 4: Sample results of stall neural approximation

Table 5 shows that the neural regression of β via equation 32 accurately estimates the propulsion characteristic to distinguish the requirement for low or high β.

Airframe	m	M	T_{engine}	Engine	β		ε
					Actual	Neural	
GR. Mk 7	8.70E+03	0.98	1.06E+05	Pegasus 11-61	1.20	1.20	0.00%
Eurofighter2000	2.10E+04	2	6.00E+04	EJ200	0.40	0.40	0.00%
A340-200	2.75E+05	0.86	1.39E+05	CFM56-5C2	6.60	5.90	10.61%

Table 5: Sample results of bypass neural approximation

No errors are attributed to the estimation of GR. Mk 7 and the Eurofighter 2000 based on an identical neural network training data entry. It is found that if the network becomes more reliant on T_{engine} by the adjustment of the adaptive parameter, better results are produced. It is expected that the inclusion of other engine performance parameters such as fuel consumption may enhance the overall accuracy of β neural approximation.

In the neural interpolation of d, sample results of Table 6 convincingly show that equation 33 is a good estimator for geometric sizing with respect to the design airframe. Note that the magnitude of errors of the last two entries implies the coverage of training data is less competent in speculating with thrust input that are too high or too low.

Engine	T_{engine}	β	d		ε
			Actual	Neural	
AL-7F	8.82E+04	0.00	1.25	1.18	5.64%
AL222-25KFK	3.01E+04	1.19	0.81	0.86	6.48%
CF6-50	2.34E+05	4.31	2.67	2.46	7.62%
F404-402	7.87E+04	0.27	0.88	0.97	10.37%
JT9D	1.93E+05	5.00	2.43	2.15	11.25%
RB.145	1.62E+04	0.00	0.53	0.61	15.23%
Trent 970	3.11E+05	8.50	2.95	2.47	16.03%
J85-5H	1.71E+04	0.00	0.52	0.61	17.84%

Table 6: Sample results of diameter neural approximation

5.3 Flight Mechanics

The determination of takeoff thrust is a critical step towards the selection of a deployment system. Hence, the numerical method from section 4.4 is verified with three sample results, collectively presented in Table 7, where D^2 calculations are shown in gray. Note that $T_{optimal}$ is the minimum thrust required with thrust vectoring at takeoff; $\tau_{optimal}$ is the respective optimum angle. Result of sample A reveals that the numerical solution of takeoff is within 2.45% margin from the reference literature [6]. This magnitude of error is solely contributed by the difference in numerical modeling methods. Meanwhile, the same calculation of the inputs from sample B indicates an optimal thrust pitch angle of 15 ° is predicted to save 15.7% of thrust relative to the non pitching design. Data of sample C is obtained from appendix A.3.1, which simulates the vectored takeoff of the Sea Harrier at a ground roll of 305m. The takeoff profile is found in

Figure 21. Note that the estimated $T_{optimal}$ is significantly less than the $T_{reference}$, as the propulsion system is capable of providing vertical takeoff. Although $\tau_{reference}$ is not available. This result further ensures that equation 17 is reliable model for optimum takeoff.

	A†	B‡	C
m	2.18E+05	3.31E+04	1.19E+04
$\hat{c}_L$	1.60	1.86	—
$\breve{c}_D$	0.05	0.03	0.03
S	325.16	88.26	18.68
v_{stall}	—	—	58.72
$X_{takeoff}$	2557.27	683.36	305.00
$\tau_{reference}$	12.00	0.00	—
$\tau_{optimal}$	10.00	15.00	33.00
$T_{reference}$	4.45E+05	1.11E+05	9.08E+04
$T_{optimal}$	4.56E+05	9.33E+04	6.91E+04
ε	2.43%	15.72%	23.87%

$\varepsilon=(T_{reference}-T_{optimal})/T_{reference}$

† [6], ‡ [26]

Table 7: Takeoff thrust vectors

The takeoff performances of type *U* and *C* engine configurations are simulated based on experimental data of the respective configurations. Results are found in 0A.5.

The simulation of landing performance is evaluated in Table 8, referenced to a sample solution [6]. This, again, shows a numerical error magnitude of about 5%.

W	1.27E+05
$\breve{c}_{D,takeoff}$	0.10
S	325.16
$v_{touchdown}$	62.16
$X_{takeoff}$	277.37
$T_{optimal}$	3.11E+05
$\tau_{optimal}$	22.00
$T_{optimal}$	2.94E+05
$\tau_{optimal}$	21.80
ε	5.57%

Table 8: Sample result of landing simulation

Table 9 shows the thrust requirements of a sample list of vehicles. Note $T_{required}$ and $T_{equipped}$ follow the definitions of equation 16 and 29, respectively. The conventional takeoff thrust and the vectored takeoff thrust are known as $T_{takeoff}$ and $T_{optimal}$. It would be expected that $T_{equipped}$ is slightly above $T_{required}$, based on the idealisation of flight mechanics analyses. This is not apparently so, possibly due to the pessimistic approximation of subsonic drag from equation 13. In the case of Aska, an excess amount of engine thrust may be equipped for

experimentation purposes. Generally, results of equation 14 are shown to accurately estimate the thrust required for various types of aerial vehicles.

Airframe	$T_{equipped}$	T_{mach}	$T_{ceiling}$	$T_{takeoff}$	$T_{optimal}$	$T_{landing}$	$T_{required}$	ε
A380-800	1.29E+06	1.33E+06	1.17E+06	1.12E+06	5.49E+05	0	1.33E+06	2.41%
Harrier AV-8B	9.62E+04	---	---	9.62E+04	9.62E+04	0	9.62E+04	0.02%
HondaJet	1.35E+04	1.32E+04	1.19E+04	1.06E+04	1.03E+04	0	1.32E+04	2.00%
Su-30	1.94E+05	---	---	---	2.12E+05	1.22E+04	2.12E+05	9.40%
Aska	1.53E+05	4.39E+04	3.25E+04	6.19E+04	3.80E+04	0	6.19E+04	59.66%

$$\varepsilon = (T_{equipped} - T_{required}) / T_{equipped}$$

Table 9: Thrust requirements of selected aerial vehicles

Figure 26 and Figure 27[a] attempts to demonstrate the best design region of the D², shown by the resultant error between the statistic and the calculated thrusts. Relationships are drawn with respect to design weights and to flight Mach numbers. The two charts indicate that D² is relatively more reliable in modeling larger vehicles, and vehicles at high supersonic speed, as there are limited numbers of vehicle types in those design regimes. At lower values of W and M, D² reveals higher error margins as there exists different vehicle types possessing different flight characteristics. Approximation of $\hat{c}_L$ and $\breve{c}_D$ may be improved by the classification of vehicle types. This is clearly the case for the calculation of T_{mach}, as it is predominately determined by $\breve{c}_D$. The rough estimation provided by equation 13 has produced errors of up to 50%, detrimental to the performance of D². In cases where the vehicle T_{mach} is falsely portrayed, it is necessary calculate engine specifications based only on $T_{takeoff}$. Another source of error is through the estimation of flight parameters via neural regression network is clearly shown on each of the charts, at magnitudes up to 33%. Thirdly, the idealisation of flight mechanics analyses have led to a general underestimation of $T_{required}$, as most points appear in the positive sector of the charts. In respect, the negative values indicate that the propulsion system is oversized, as defined by $\varepsilon = (T_{equipped} - T_{calculated}) / T_{equipped}$.

[a] Based on the tabulated results found in A.4.

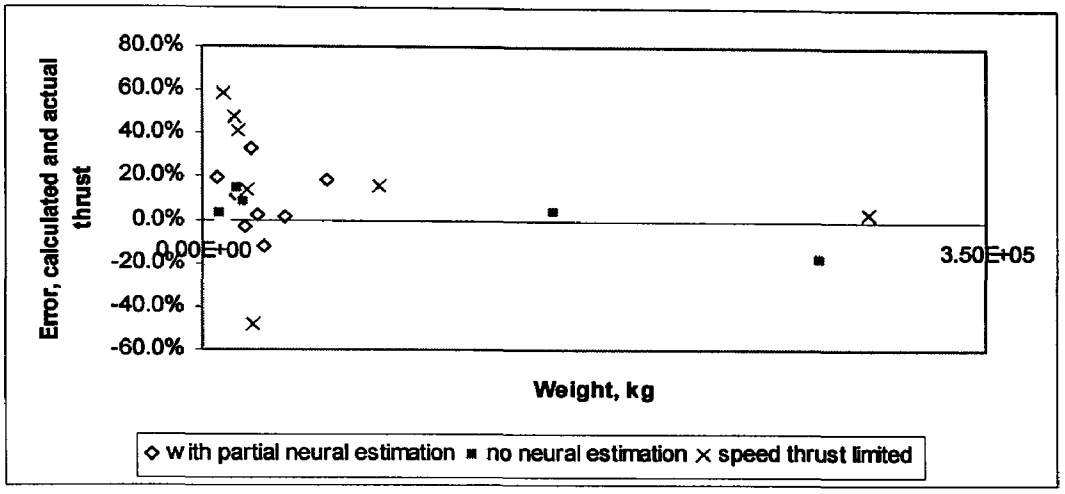

Figure 26: Analysis of errors the calculation of thrust requirement in relation to the design weight

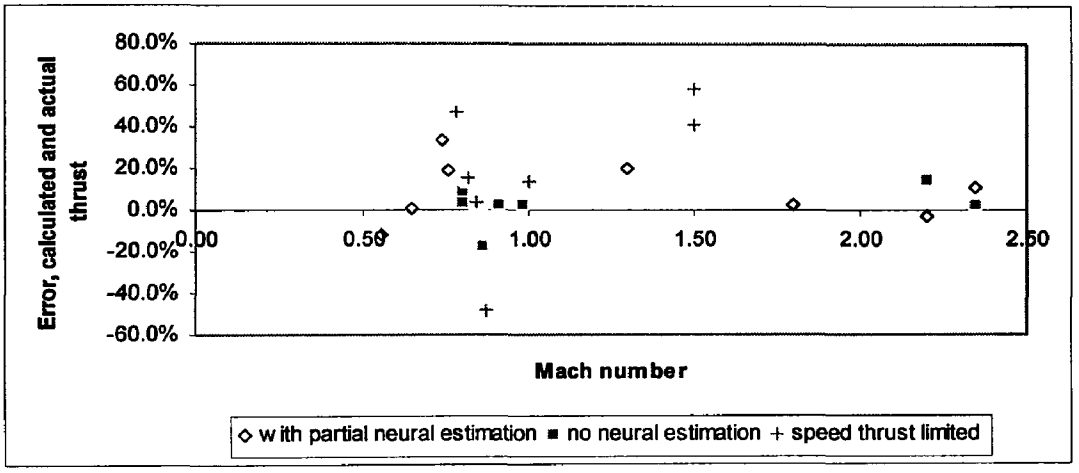

Figure 27: Analysis of errors the calculation of thrust requirement in relation to the design Mach number

5.4 Engine Sizing

In determining the validity of the engine sizing process introduced in section 4.5 and to integrate results of D^2, the following are case analyses of three vehicle types. Calculated results are highlighted as gray.

Table 10 compares two calculations against the primary inputs based on A380-800. Solution 1 shows that the wing area, if wrongly estimated, results in a significant deviation of $T_{required}$. Meanwhile, other output parameters are portrayed fairly accurately via neural approximations

	A380-800		
m	5.60E+05		
M	0.89		
Z	13100		
$X_{takeoff}$	2050		
$X_{landing}$	2900		
	Actual	Solution1	Solution2
S	845.00	*628.00*	845.00
v_{stall}	—	*64.81*	*64.81*
$\Lambda_{selected}$	Conventional	Conventional	Conventional
n	4	4	4
m_{engine}	—	5.19E+03	5.36E+03
d	2.95	*2.69*	2.95
β	8.50	*5.79*	8.50
T_{engine}	3.11E+05	3.09E+05	3.52E+05
$T_{equipped}, T_{required}$	1.29E+06	1.12E+06	1.28E+06
ε	—	13.3%	1.2%

Italics: Neural estimations

$\varepsilon = (T_{equipped} - T_{required})/T_{equipped}$

Table 10: A380-800 case analysis

Table 11 presents comparisons between the actual and calculated results of the vertical takeoff Yak-38 and a similar AV-8 aircraft. Here, D^2 proposes a type *S* design that is similar to the Harrier. This is originated from the establishment of fuzzy rules for supersonic vehicle designs. Other quantitative results compare the actual data with reasonable amount of precision.

	Yak-38, Yak-36M		Harrier AV-8B
m	1.03E+04		9.34E+03
M	0.96		0.98
Z	12002		15600
$X_{takeoff}$	0		0
$X_{landing}$	0		0
	Actual	Solution	Actual
S	18.49	18.49	21.37
v_{stall}	0.00	0.00	0
$\Lambda_{selected}$	Dual	Single	Single
n	1[1]	1	1
m_{engine}	—	2.06E+03	1.93E+03
d	—	1.23	1.22
β	0	1.20	1.2
T_{engine}	4.90E+04	1.17E+05	1.06E+05
$T_{equipped}, T_{required}$	1.06E+05[1]	1.06E+05	9.67E+04
τ	—	-90	-90
ε	—	0.5%	—
$T_{landing}$	—	1.06E+05	9.62E+04

[1] total of 1 thrust engine and 2 lift engines

$\varepsilon = (T_{equipped} - T_{required})/T_{equipped}$

Table 11: Yak-38 case analysis

The calculated thrust of the HondaJet is very close to the actual value. The output of the neural approximated parameters are congruent with similar vehicles of the same type. However, D² has produced a type *S* engine unit. In actual design, a two unit design reduces engine acoustics to the airframe. However, such design consideration is not included in the fuzzy configuration model. Results are presented in Table 12.

	HondaJet	
m	4.17E+03	
M	0.73	
Z	12497	
$X_{takeoff}$	807	
$X_{landing}$	694	
	Actual	Solution
S	—	*21.00*
v_{stall}	—	*46.30*
$\Lambda_{selected}$	—	Single
n	2	1
m_{engine}	—	3.62E+02
d	—	*0.56*
β	—	*0.90*
T_{engine}	7.43E+03	1.17E+04
$T_{equipped}, T_{required}$	1.35E+04	1.06E+04
τ	—	11.4
ε	—	21.4%
$T_{landing}$	—	0

Italics: Neural estimations

$$\varepsilon = (T_{equipped} - T_{required}) / T_{equipped}$$

Table 12: HondaJet case analysis

6 CONCLUSION

The development of the expandable engineering expert system E^3 and the deployment design process D^2 have been presented in this study. The development combined elements of AI and existing airplane design knowledge. The resultant new design approach has been evaluated at different levels. It is found that the use of fuzzy classification of airplane types have accurately portrayed actual designs. Despite the inherent numerical uncertainties from data sources, the use of neural network regression in predicting flight characteristics is precise and efficient, in which it supports further analysis of performance requirement of the propulsion system. Numerical simulation results of takeoff and landing were verified with referenced sources. Calculations of gross thrust reveal that D^2 produces the most accurate engine specifications based on the deployment requirements of takeoff, in which this study is dedicated to accomplish. Overall, the output parameters clearly describe the deployment systems at the expense of five primary input parameters, making D^2 an economical design process. The design case studies of various vehicle types have further proven D^2, in which the capabilities of the expert system E^3 was effectively utilised. E^3 itself has demonstrated the versatility in managing knowledge in various forms. This asset is crucial for modifications and interdisciplinary problem solving. This is based on the simple, yet organisational, expert system platform and AI analysis tools provided by Matlab and developed in this study.

As with most computational analyses, more accurate data would have positive effects on the results of D^2. This will enable more sophisticated design process knowledge to be implemented. It is hypothesised that the categorisation of vehicle types prior to data or flight mechanics calculations may significantly improve the error margin to less than 20%. This is based on the low error margins of results found on the remote areas of the x axes in Figure 26 and Figure 27. The process of categorisation may involve modification of the existing fuzzy module with additional inputs and outputs.

Although presented as an open loop design process, the logical sequence of D^2 may be modified to incorporate other design factors. For example, FAR[a] 23 states that single engine light vehicles must have an upper limit of stall speed. This statement can only be verified after the engine sizing sequence. Thus, this can be implemented as in Figure 28.

---

[a] Federal Aviation Regulation

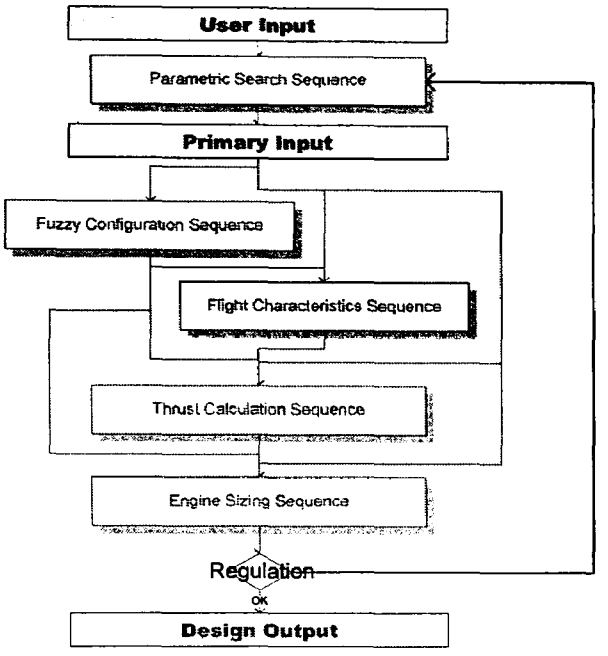

Figure 28: Modification of D^2

With sufficient support of a reliable data bank, D^2 may be extended to the inclusion of other aerial vehicle design analyses, incorporating more design variables to address the final design more accurately. This study has provided meaningful results for further researches of similar disciplines, from the perspective of investigating the integration of different AI elements into aerial vehicle design.

While D^2 is an expert system process dedicated to the design of airplane deployment systems, the general expert system environment E^3 is not limited to one or one type of engineering problem. Potential capabilities of the parametric search module, the organisation of files and variables have not fully exploited in this study. The available AI may be used or enhanced in a number of ways:

- Fully automate the design process via the parametric search module
- Present solution options throughout the execution of the parametric search module
- Develop fuzzy systems based on the pattern recognition capability of neural networks, i.e. Neurofuzzy systems

To further advance the development of the expert system design process, proper interfacing is essential with other engineering software, such as finite element analysis, simulation, computer assisted design, etc. This, if applied, will ultimately benefit engineering research, development as a practical or training tool.

REFERENCES

1. Tzafestas, Spyros. Expert Systems in Engineering Applications. Springer-Verlag, 1993.
2. Kowalski, Zbigniew. et al. An Expert System for Aided Design of Ship Systems Automation. Expert Systems with Applications 20. Elsevier Science Ltd. 2001.
3. Nah, Seung-Hyeog. DESAID (The Development of an Expert System for Aircraft Initial Design). Ph.D Dissertation, College of Aeronautics, Cranfield Institute of Technology. 1991.
4. Li, Shuixiang; Qiao, Minggao. A hybrid expert system for finite element modeling of fuselage frames. Expert Systems with Applications 24, 2003. p87.
5. Shaalan, Khaled; Rizk, Mohammed; Abdelhamid, Yasser; Bahgat, Reem. An expert system for the best weight distribution on ferryboats. Expert Systems with Applications 26, 2004. p397.
6. Gilyard, Glenn B.; Bolonkin, Alexander. Optimal Pitch Thrust-Vector Angle and Benefits for all Flight Regimes. NASA TM-2000-209021. 2000.
7. Roskam, Jan. Airplane Design Volume I & II. 1985.
8. Kohlman, David L. Introduction to V/STOL Airplanes. The Iowa State University Press. 1981.
9. Piccirillo, Albert C. German V/STOL Fighter Program: A Quest for Survivablility in a Nuclear Theatre Environment. AIAA, USA. 1997.
10. Hirschberg, Michael J. Soviet V/STOL Aircraft: The Struggle for a Shipborne Combat Capability. AIAA, USA. 1998.
11. Deckert, W. H.; Franklin, J. A. Powered-Lift Aircraft Technology. NASA SP510. 1989.
12. Braybrook. V/STOL The Key To Survival. Osprey Publishing Limited, London. 1989.
13. http://www.nal.go.jp/ndivision/flight/japanese/Museum/ASKA/aska.html. 07 Jan 2005.
14. Federation of American Scientists. URL: www.fas.org. 07 Jan 2005.
15. Takanashi, Susumu; Sawada, Keisuke. Numerical Simulation of Compressible Flow Field about Complete ASKA Aircraft Configuration. International Powered Lift Conference. Santa Clara, California. Society of Automotive Engineers P-203. 1987.
16. Wickens, R. H. The Spanwise Lift distribution and trailing vortex wake downwind of an externally blown jet-flap. V/STOL Aerodynamics. AGARD Conference N143. AGARD-CP-143. 1974.
17. Phelps, Arthur E. III. Aerodynamics of the Upper Surface Blown Flap. STOL Technology Conference. NASA. 1972.
18. Moorhouse, David J. Predicting the Maximum Lift of Jet-Flapped Wings. V/STOL Aerodynamics. AGARD Conference N143. AGARD-CP-143. 1974.
19. Bucknell, R. L. STOVL Engine/Airframe Integration. AIAA/SAE/ASME/ASEE 23th Joint Propulsion Conference. 1987.
20. Lewis, W. J.; Simpkin, P. A Comparision of Propulsion Systems for V/STOL Supersonic Combat Aircraft. Society of Automotive Engineering 801141. 1980.

21. MATLAB 6, Mathworks.
22. Martin, James et al. Building Expert Systems, A Tutorial. Prentice Hall Englewood Cliffs. New Jersey, 1988.
23. Kasabov, Nikola K. Foundations of Neural Networks, Fuzzy Systems, and Knowledge Engineering. The MIT Press. USA. 1996.
24. Wesley, Hines J. Matlab Supplement to Fuzzy and Neural Approaches in Engineering, John Wiley & Sons, Inc. New York., 1997.
25. www.rolls-royce.com/defence_aerospace/products/combat/pegasus/default.jsp 07Jan 2005.
26. Anderson, John. Aircraft Performance and Design. WCB McGraw-Hill. 1999. USA.
27. Yamato, Hiroyki; Okada, Noriaki; Bando, Toshio. Flight Test of the Japanese Upper Surface Blowing STOL Experimental Aircraft ASKA. AIAA 4th Flight Test Conference, San Diego. 1988.
28. Jane, F. T. Jane's All The World's Aircraft 2002-2003.
29. Jane, F. T. Jane's All The World's Aircraft 2003-2004.

A APPENDIX

A.1 List of Matlab Programs and Excel Data Files

Expert System Files	
MainThing.fig	Graphical user interface of DSquare
bb2p.m	Dissociate the blackboard variables from Matlab to ECube form
dSquare5.m	Engine sizing sequence of DSquare
dSquare234.m	Fuzzy, regression, and flight mechanics sequences of DSquare
MainThing.m	Controller of MainThing.fig
NeuralRegress.m	Generate a neural regression network from an input of training database
pList.m	Generate a list of all input and output parameters from all subroutines
RagnarokFix.m	Test version of DSquare
Refuzzify.m	Reproduce membership categorisation by refuzzifying the fuzzy output quantities
sBackward.m	Proposed algorithm for finding subroutine solution based on unknown parameters, incomplete
sForward.m	Algorithm for finding subroutine solution based on known parameters
sList.m	Generate a list of all subroutines and their respective I/O parameters
SplitMatrix.m	Matrix operation algorithm for NeuralRegress.m
sSquare.m	Executes solution based on sForward.m

Subroutine Files	
AltitudeCondition.m	Deduces altitude temperature, pressure and density
CeilingThrust.m	Finds the thrust required to achieve service ceiling [26]
EmptyMaxWeight.m	Estimates the maximum takeoff weight via empty weight
EngineSpecs.m	Determines the propulsion system to meet the required thrust
FuzzySpecs.m	Engine configuration selection
LandingLength.m	Calculates the required landing ground roll [6]
LandingThrustVector.m	Calculates the minimum landing ground roll required via thrust vectoring [6]
LLift.m	Calculates the lift increase from the thrust exhaust below wing via wind tunnel model [20]
CTakeoffLength.m	Calculates the takeoff length of type C vehicle
CTakeoffThrust.m	Calculates thrust to takeoff via conventional engine deflection model
MachThrust.m	Finds the sealevel thrust to attain the mach speed specified altitude [26]
NeuralArea.m	Finds wing area via generalised neural training of samples
NeuralAspect.m	Finds aspect ratio based on generalised neural training of samples
NeuralBypass.m	Finds engine bypass ratio via generalised neural training of samples
NeuralDiameter.m	Finds engine diameter via generalised neural training of samples
NeuralStall.m	Finds stall speed via generalised neural training of samples
SpeedMach.m	Converts speed to mach via altitude temperature
StallLiftmax.m	Finds the maximum lift coefficient based on a specified stall speed
TakeoffLength.m	Finds the required takeoff length [6]
TakeoffThrust.m	Finds the thrust required to takeoff
TakeoffThrustVector.m	Finds minimum takeoff thrust and respective thrust angle [6]
ThrustCriterion.m	Sets engine thrust limit to the maximum found in a database of engines
ULift.m	Calculates an increase of lift due to upper surface blowing based on Aska flight data [27]
UTakeoffLength.m	Solves for the required takeoff length for upper configuration type vehicles
UTakeoffThrust.m	Finds thrust required to takeoff for upper configurations
WeightCriterion.m	Suppress weight of all engines to below a weight ratio or an offset of
EngineConfig.fis	Fuzzy inference system of engine configuration selection

Data Files	
AIRFRAMES.xls	Database of thrust and power based vehicles
ENGINES.xls	Database of thrust and power based engines
EmptyMaxWeight.xls	Linear relationship between empty and maximum weight of vehicles
LinearEngine.xls	Linear relationships to support EngineSpecs.m
LinearLiftMax.xls	Models upper and conventional engine configurations based on extrapolation of data
NeuralArea.xls	Test and training data for NeuralArea.m
NeuralAspect.xls	Test and training data for NeuralAspect.m
NeuralBypass.xls	Test and training data for NeuralBypass.m
NeuralDiameter.xls	Test and training data for NeuralDiameter.m
NeuralStall.xls	Test and training data for NeuralStall.m
InputFile.xls	Provides the inputs for RagnarokFix.m

A.2 Empty VS Maximum Vehicle Weight

The relationship below is used to project the maximum takeoff based on the empty vehicle weight. Data is made up of both power and thrust rated propulsion system found in A.3.1. A linear regression line is drawn, intercepting at the origin.

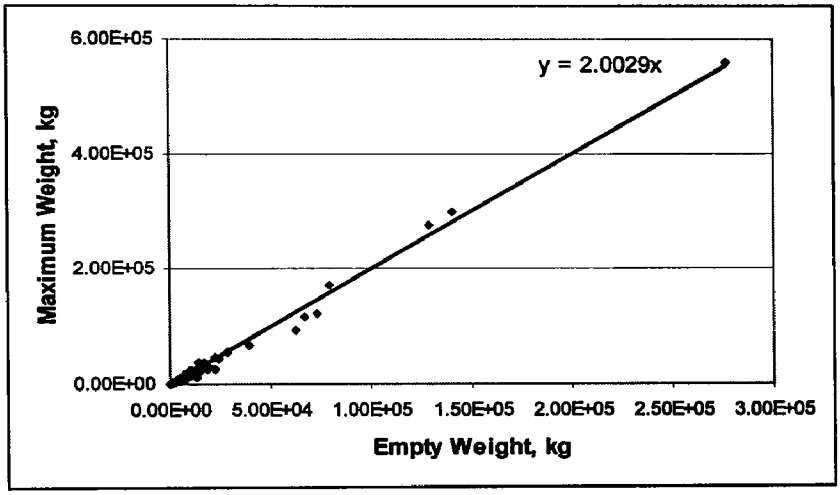

Maximum takeoff weight versus empty weight of vehicles

A.3 Data

A.3.1 Airframes

Airframe	m	M	Z	$X_{takeoff}$	$X_{landing}$	σ	S	v_{stall}	nT_{engine}	n	Engine	m_{empty}
767-200ER	1.56E+05	0.80	11550	2071	1372	8.00	283.30	63.43	4.50E+05	2	—	—
777-200ER	2.98E+05	0.84	13137	3030	1630	8.70	427.80	65.05	8.30E+05	2	Trent 895	1.40E+05
A300-600R	1.71E+05	0.82	12000	1890	1166	7.70	260.00	62.96	5.48E+05	2	CF6-80C2	7.93E+04
A318	6.60E+04	0.82	11890	1670	1332	9.50	122.60	—	2.14E+05	2	PW6124	3.90E+04
A340-200	2.75E+05	0.86	11887	3017	1890	10.10	361.60	68.42	5.55E+05	4	CFM56-5C2	1.30E+05
A380-800	5.60E+05	0.89	13100	2050	2900	7.50	845.00	—	1.42E+06	4	Trent 970	2.77E+05
AMX	1.08E+04	0.86	13000	631	464	3.80	21.00	—	4.91E+04	1	Spey 807	6.73E+03
An-124	4.05E+05	0.81	12000	2520	900	8.60	628.00	64.81	—	—	—	—
An-72	2.75E+04	0.56		620	420	10.30	98.53	—	1.27E+05	2	D-36	1.91E+04
An-72	3.30E+04	0.65	10100	620	420	10.30	98.53	50.00	1.27E+05	2	D-36	1.91E+04
An-74	3.65E+04	0.65	10210	930	465	10.30	98.53	—	1.27E+05	2	D-36 2A	—
An-74T-300	3.45E+04	0.59	—	—	—	—	98.62	—	1.27E+05	2	D-36 4A	—
Aska	3.87E+04	0.57	6096	578	408	7.77	120.00	31.48	1.69E+05	4	FJR 710/600S	—
AT-63 PAMPA	5.00E+03	0.80	12900	430	460	6.01	15.63	42.22	1.56E+04	1	TFE731-2C-2N	2.82E+03
C-17A	2.65E+05	0.77	13715	2124	824	7.20	353.03	59.16	7.20E+05	4	F117-PW-100	—
DO-31*	2.74E+04	0.60	10515	—	—	5.72	57.00	—	1.91E+05	2	Pegasus	2.25E+04
Eurofighter 2000	2.10E+04	2.00	—	300	—	2.40	50.00	—	1.20E+05	2	EJ200	1.00E+04
F-15E	3.67E+04	2.50	—	—	—	3.00	56.49	—	2.09E+05	2	F100-220	1.45E+04
F-18E	2.99E+04	1.80	15240	—	—	4.00	46.45	57.87	1.96E+05	2	F414-400	1.40E+04
F-2	2.21E+04	2.00	—	—	—	3.30	34.84	—	1.31E+05	1	F110-129	9.63E+03
F-22	2.72E+04	1.70	15240	—	—	2.40	78.00	—	3.12E+05	2	F119-100	1.44E+04
F-35	2.08E+04	1.60	—	—	—	2.68	42.70	0.00	8.90E+04	1	F135	1.36E+04
F-8 IIM	1.89E+04	2.20	18000	630	900	—	—	83.33	1.36E+05	2	—	1.04E+04
Falcon 900	2.22E+04	0.87	15500	1590	724	7.60	49.00	54.44	6.34E+04	3	—	—
GR. Mk 7	8.70E+03	0.98	15600	0	0	4.00	21.37	0.00	1.06E+05	1	Pegasus 11-61	7.05E+03
Harrier AV-8B	9.34E+03	0.98	15600	0	0	4.00	21.37	0.00	1.06E+05	1	Pegasus 11-61	6.34E+03
Harrier AV-8B	1.41E+04	0.98	15600	—	—	4.00	21.37	0.00	1.06E+05	1	Pegasus 11-61	6.34E+03
HondaJet	4.17E+03	0.73	12497	807	694	—	—	—	1.49E+04	2	HF118	—
J-7E	9.10E+03	2.35	17500	700	700	2.78	24.88	72.02	6.47E+04	1	WP13F	5.29E+03
J-8 II	1.53E+04	2.20	20200	670	1000	2.07	42.20	80.25	1.32E+05	2	WP13A	9.82E+03
Jaguar	1.57E+04	1.50	13715	1250	680	3.10	24.18	59.16	7.48E+04	2	Adour Mk 811	7.00E+03
Jas-39A	1.40E+04	1.00	15239	800	600	—	—	51.44	8.05E+04	1	F404-400	8.00E+03
JH-7	2.85E+04	1.70	15600	920	1050	3.09	52.30	—	1.82E+05	2	Spey 202	—
K-8	4.33E+03	0.75	13600	410	512	5.40	17.02	44.44	—	—	—	—
Legacy B	2.00E+04	0.78	11887	1759	818	—	—	—	6.60E+04	2	AE 3007A1P	1.19E+04
Leopard B	1.81E+03	0.80	15545	—	641	8.80	5.85	43.33	6.22E+03	2	FJX-2	8.62E+02
Mako	9.40E+03	1.50	14400	450	750	2.60	26.70	—	9.00E+04	1	EJ200	6.20E+03
MiG AT	7.80E+03	0.80	15500	540	570	—	17.67	48.35	—	—	—	—
MiG-21PD*	—	—	—	198	250	—	—	—	1.11E+05	1	R-13-300	—
MiG-23	1.47E+04	2.35	18500	500	750	1.62	37.35	—	1.28E+05	1	R-35-300	1.02E+04
MiG-23PD	1.85E+04	—	—	—	—	1.49	40.00	—	9.50E+04	1	R-27-300	—
MiG-25RB	4.12E+04	2.83	21000	1250	800	—	61.40	77.67	—	—	—	—
MiG-29	2.24E+04	1.01	17500	—	—	3.40	42.28	—	1.71E+05	2	RD-33	—
MiG-31	4.62E+04	2.83	20600	1200	800	2.90	61.60	72.53	1.86E+05	2	D-30F6	2.18E+04
Mirage 2000 5	1.75E+04	2.20	18290	—	—	2.03	41.00	64.44	9.51E+04	1	M53-P2	7.50E+03
Mirage III V*	1.36E+04	2.04	—	0	0	—	—	0.00	2.73E+05	1	TF-30	—
Rafale	2.45E+04	1.80	16765	600	—	2.60	45.70	61.73	1.77E+05	2	M88-3	1.06E+04
RJ100	4.60E+04	0.73	10670	1184	1014	9.00	77.29	48.89	—	—	—	—
RJ70	4.31E+04	0.73	10670	983	1062	9.00	77.29	47.78	1.24E+05	4	—	2.39E+04
RJ85	4.40E+04	0.73	10670	1043	951	9.00	77.29	47.78	—	—	—	—
Sea Harrier	1.19E+04	1.25	15600	305	0	3.17	18.68	—	9.56E+04	1	Pegasus 106	6.37E+03
Su-25	1.76E+04	0.80	17000	500	650	6.10	33.70	55.56	8.84E+04	2	R-195	9.70E+03
Su-27IB	4.44E+04	1.80	15000	—	—	3.50	62.00	—	3.50E+05	2	AL-41F	—
Su-33	3.30E+04	2.16	17000	195	—	3.20	67.84	—	1.50E+05	2	AL-31F3	—
Su-35	3.88E+04	2.35	17200	960	—	3.50	62.04	—	2.46E+05	2	AL-31FP	1.70E+04
T-4	7.50E+03	0.91	14815	655	704	4.70	21.00	46.30	3.27E+04	2	F3-30	3.84E+03
Tu-234 LR	1.03E+05	0.80	12600	2050	2050	9.60	182.40	56.48	3.17E+05	2	—	—
Tu-234	8.48E+04	0.80	12600	1450	2050	9.60	182.40	55.09	3.17E+05	2	—	—
Typhoon	2.30E+04	2.00	16765	300	700	2.40	50.00	—	1.80E+05	2	EJ200	1.10E+04
VAK 191B*	7.50E+03	0.90	—	0	0	3.04	12.50	0.00	9.48E+04	1	RB.193-12	5.27E+03
VJ-101C	6.60E+03	1.30	12000	0	0	—	—	0.00	9.74E+04	6	RB.145	5.40E+03
X-14	1.41E+03	—	—	0	0	—	—	0.00	1.56E+04	2	ASV8 Viper	—
X-32B	2.27E+04	1.50	—	—	—	1.66	50.00	0.00	—	1	JSF119-614S	9.98E+03
X-50	6.00E+02	0.58	3050	0	0	—	—	0.00	—	1	F112	—
Yak-130	9.00E+03	0.99	13000	340	550	4.00	23.52	45.83	4.90E+04	2	RD-2500	4.60E+03
Yak-36	9.40E+03	0.94	12002	0	0	4.24	15.98	0.00	9.80E+04	2	R-27-300	5.60E+03
Yak-38*	1.03E+04	0.96	12002	0	0	2.90	18.49	0.00	1.06E+05	1	R-27-300	7.48E+03
Yak-38M*	1.13E+04	0.96	12002	0	0	2.90	18.49	0.00	1.29E+05	1	R-28V-300	8.39E+03
Yak-38U*	1.00E+04	0.96	12002	0	0	2.90	18.49	0.00	1.06E+05	1	R-27-300	8.39E+03
Yak-41*	1.95E+04	1.70	14935	99	244	3.22	31.70	0.00	2.32E+05	1	R-79V-300	1.17E+04
YC-14	7.71E+04	0.60	13716	572	610	—	163.70	—	4.54E+05	2	CF6-50D	—
YC-15	7.01E+04	0.80	9144	610	610	—	—	—	2.84E+05	4	JT8D-17	—

Airframe	m	M	Z	$X_{takeoff}$	$X_{landing}$	σ	S	v_{stall}	nP_{engine}	n	Engine	m_{empty}
206L-4	2.02E+03	0.17	3050	0	0	0.00	0.00	0.00	9.70E+04	1	250-C30P	1.05E+03
23F	8.80E+00	0.05	2285	0	0	0.00	0.00	0.00	8.58E+03	1	Zenoah	5.90E+00
430 A	4.22E+03	0.21	5590	0	0	0.00	0.00	0.00	2.34E+06	2	250-C40B	2.42E+03
60F	1.81E+01	0.07	2285	0	0	0.00	0.00	0.00	--	--	--	9.10E+00
665	6.10E+03	0.19	3200	0	0	0.00	0.00	0.00	3.83E+06	2	--	4.20E+03
706 Seabat	9.07E+01	0.31	1050	0	0	0.00	0.00	0.00	--	1	AR 731	5.22E+01
A160 Hummingbird	1.81E+03	0.24	9145	0	0	0.00	0.00	0.00	2.98E+05	1	Leading Systems	--
A400M	1.17E+05	0.72	11280	1402	625	8.10	221.50	66.87	3.58E+07	4	BR 715	6.65E+04
ACRW	1.36E+02	--	--	0	0	--	--	0.00	2.83E+04	1	AR 741	--
AH-1W	6.69E+03	0.23	4270	0	0	0.00	0.00	0.00	5.14E+05	2	T700-401	4.95E+03
AH-64	1.04E+04	0.23	5915	0	0	0.00	0.00	0.00	5.79E+06	2	T700-701C	5.35E+03
An-140	1.92E+04	0.51	7200	1148	1148	--	--	--	3.68E+06	2	--	--
An-70	1.23E+05	0.76	11000	1800	1900	--	--	--	4.16E+07	4	D-27	7.28E+04
APID 2	5.50E+01	0.08	300	0	0	0.00	0.00	0.00	9.17E+03	1	K-100	3.50E+00
ARCH-50	3.00E+02	0.08	100	0	0	0.00	0.00	0.00	4.85E+04	1	586	2.38E+02
BA609	7.27E+03	0.46	7620	0	0	--	--	0.00	2.89E+06	--	--	4.77E+03
Beech 1900D	7.77E+03	0.45	7620	968	705	10.90	28.80	43.33	1.91E+06	2	--	--
BK117-B2	3.50E+03	0.23	5090	0	0	0.00	0.00	0.00	2.64E+05	2	1E2	1.76E+03
BRT-8 Dervish	2.00E+01	--	--	0	0	0.00	0.00	0.00	--	--		5.60E+01
C-130J	7.03E+04	0.59	9315	930	427	10.10	162.12	51.39	1.37E+07	4	--	--
Camcopter Mk 2	6.80E+01	0.08	3810	0	0	0.00	0.00	0.00	2.83E+04	1	AR 741	4.30E+01
CH-47	2.45E+04	0.24	3385	0	0	0.00	0.00	0.00	1.12E+07	2	T55-L-712	1.16E+04
CL-227 Sentinel	2.27E+02	0.12	3000	0	0	0.00	0.00	0.00	4.47E+04	1	WTS125	1.11E+02
CL-327 Guardian	3.50E+02	0.14	5485	0	0	0.00	0.00	0.00	9.32E+04	1	WTS117-5	1.50E+02
CL-427	3.40E+02	0.19	5485	0	0	0.00	0.00	0.00	9.32E+04	1	WTS117-5	1.35E+02
Copter 1	--	--	200	0	0	0.00	0.00	0.00	--	--	--	6.40E+00
Copter 2	--	0.07	500	0	0	0.00	0.00	0.00	--	--	--	8.00E+00
Cypher	1.13E+02	0.11	2440	0	0	0.00	0.00	0.00	3.80E+04	1	AR 801	7.50E+01
DA 20-C1	7.50E+02	--	--	337	377	--	11.60	17.50	--	--	--	--
Dornier 228	6.40E+03	0.34	8535	442	343	9.00	32.00	32.50	4.26E+06	2	TPE331-5-252D	3.69E+03
DP4	6.35E+01	0.13	2135	0	0	0.00	0.00	0.00	1.27E+04	1	QA-200XL	3.18E+01
Dornier Seamos	1.13E+03	0.14	3660	0	0	0.00	0.00	0.00	3.36E+05	1	250-C20R	5.95E+02
Eagle Eye	1.02E+03	0.34	6100	0	0	--	--	0.00	3.36E+05	--	250-C20R	--
EH101	1.46E+04	0.25	4575	0	0	0.00	0.00	0.00	9.40E+06	3	RTM 322-01/8	1.05E+04
EMB-314	3.19E+03	0.37	10670	350	550	6.40	19.40	43.61	1.94E+06	1	PT6A-68	2.42E+03
Eurofar	1.37E+04	0.52	3050	0	0	--	--	0.00	6.40E+06	2	--	--
EV-97	4.50E+02	--	--	145	--	--	9.84	18.52	5.96E+04	--	--	--
Heliot	4.50E+02	0.12	2050	0	0	0.00	0.00	0.00	7.83E+04	1	F30A26AK	2.30E+02
Heliwing	6.58E+02	0.16	4575	0	0	--	--	0.00	1.79E+05	1	WTS124	--
HK 36 TC	7.70E+02	0.17	--	201	--	17.43	15.30	0.00	1.19E+05	1	912A-3	5.55E+02
Hokum-X	4.08E+03	0.21	3350	0	0	0.00	0.00	0.00	9.62E+05	1	T53-L-703	--
IL-114	2.35E+04	--	--	1360	1260	11.00	81.90	44.44	3.68E+06	--	--	--
Ka-137	2.80E+02	0.15	3000	0	0	0.00	0.00	0.00	4.51E+04	1	2706	--
Ka-22	9.37E+04	0.29	18050	0	0	--	--	0.00	4.85E+06	1	D-25VK	6.22E+04
Ka-29	1.15E+04	0.23	4300	0	0	0.00	0.00	0.00	3.27E+06	2	TV3-117VMA	5.52E+03
Ka-37	2.50E+02	0.09	3000	0	0	0.00	0.00	0.00	4.51E+04	1	Ka-37	--
Ka-50	1.08E+04	0.26	5500	0	0	0.00	0.00	0.00	3.27E+06	2	TV3-117VMA	7.80E+03
MH2000	4.50E+03	0.24	--	0	0	0.00	0.00	0.00	2.61E+06	2	MG5-110	2.50E+03
Mi-26	5.60E+04	0.25	4600	0	0	0.00	0.00	0.00	1.70E+07	2	D-136	2.82E+04
Midget RPG MK I	2.50E+01	--	--	0	0	0.00	0.00	0.00	--	--	--	--
Midget RPG MK II	5.00E+01	0.10	50	0	0	0.00	0.00	0.00	--	--	--	--
Midget RPG MK III	9.00E+01	--	--	0	0	--	--	0.00	--	--	--	--
MV-22	2.40E+04	0.42	7925	0	--	5.50	35.49	0.00	1.83E+07	2	T406-AD-400	1.50E+04
MV-22	2.40E+04	0.42	7925	0	--	5.50	35.49	0.00	1.83E+07	2	T406-AD-400	1.50E+04
MV-22	2.74E+04	0.42	7925	152	--	5.50	35.49	--	1.83E+07	2	T406-AD-400	1.50E+04

Airframe	m	M	Z	$X_{takeoff}$	$X_{landing}$	σ	S	v_{stall}	nP_{engine}	n	Engine	m_{empty}
Q300	1.86E+04	0.48	7620	859	859	13.40	56.21	39.17	3.55E+06	2	--	--
Q400	2.93E+04	0.58	7620	1014	1094	12.80	63.08	--	7.44E+06	2	--	--
Quad Tiltrotor	4.54E+04	--	--	0	0	--	--	0.00	--	4	--	--
R-50	6.70E+01	0.02	100	0	0	0.00	0.00	0.00	8.95E+03	1	L 12	4.40E+01
RAH-66	7.90E+03	0.26	--	0	0	0.00	0.00	0.00	4.66E+05	2	T800-801	4.22E+03
RF-9	7.50E+02	--	--	360	--	16.10	18.00	19.55	5.96E+04	--	--	--
R-MAX	8.80E+01	0.02	100	0	0	0.00	0.00	0.00	1.57E+04	1	L15	5.80E+01
RoboCopter 300	7.94E+02	--	--	0	0	0.00	0.00	0.00	1.57E+05	1	TIO-360-C	4.99E+02
RPH-2 and FFOS	3.25E+02	0.10	2000	0	0	0.00	0.00	0.00	6.23E+04	1	Fuji Robin	2.05E+02
S-70A	7.48E+03	0.24	5790	0	0	0.00	0.00	0.00	5.37E+06	2	T700-701C	5.12E+03
Soar Bird	--	0.13	3000	0	0	0.00	0.00	0.00	--	--		2.80E+02
STF-9A	1.00E+02	0.24	6100	0	0	--	2.30	0.00	--	1	AR 731	7.70E+01
STF-9B	2.76E+02	--	--	0	0	--	--	0.00	8.95E+04	1	642	1.54E+02
STOL CH 701	4.99E+02	--	--	--	24	--	--	13.89	1.19E+05	1	912 UL	2.08E+02
STOL CH801	9.75E+02	0.15	4267	119	46	5.80	15.51	24.70	1.34E+05	1	O-360-A	5.22E+02
T67	1.16E+03	0.23	--	334	401	8.90	12.63	27.78	1.94E+05	1	--	--
Vigilant F 2000	1.00E+01	0.08	2000	0	0	0.00	0.00	0.00	--	--	--	2.75E+01
Vigilante 496 OPV	4.99E+02	0.19	3660	0	0	0.00	0.00	0.00	5.28E+04	1	F 30	2.74E+02
Vigilante 500	4.99E+02	0.19	3960	0	0	--	--	0.00	5.28E+04	1	F 30	2.66E+02
Vigilante 600	--	0.22	4575	0	0	--	--	0.00	1.12E+05	1	Zoche	2.84E+02
VTOL Concept	3.70E+04	0.75	12000	0	0	3.30	30.00	0.00	1.07E+07	1	--	3.70E+04
VTOL Concept	3.70E+04	0.75	12000	30	0	3.30	30.00	0.00	1.07E+07	1	--	3.70E+04
X-22A	7.71E+03	0.43	--	0	0	--	--	0.00	3.73E+06	4	YT58-GE-8D	--
XF-109	1.08E+04	--	--	--	--	2.91	18.02	--	--	1	J85-5	1.38E+04
XV-15	5.90E+03	0.53	8840	0	0	7.32	15.70	0.00	2.31E+06	2	LTC1K-4K	4.34E+03
Y-12	5.30E+03	0.28	--	230	--	8.70	--	--	--	--	--	--
Zephyr	4.50E+02	--	--	120	--	--	10.10	18.52	5.96E+04	--	--	--

A.3.2 Engines

Model	Manufacture	β	d	m	τ
TFE731	Allied Signal	--	1.02	4.48E+02	1.56E+04
F124	Allied Signal	--	0.91	4.99E+02	2.80E+04
F109-GA--00	Allied Signal	--	0.79	1.99E+02	5.92E+03
CFE 738	Allied Signal	--	1.22	6.01E+02	2.67E+04
ALF502/507	Allied Signal	--	1.27	6.12E+02	2.98E+04
ASV8 Viper	AS	--	--	--	7.78E+03
PS-90A12	Aviadvigatel	5.05	1.67	2.30E+03	1.18E+05
D-30KU	Aviadvigatel	2.42	1.56	2.67E+03	1.08E+05
D-20P	Aviadvigatel	1.00	0.98	1.47E+03	5.30E+04
CFM56-5C	CFM	6.60	1.84	2.64E+03	1.51E+05
CFM56-3	CFM	5.00	--	--	1.05E+05
CFM56-7B27s	CFM	5.10	1.55	2.38E+03	1.21E+05
EJ200	Eurojet	0.40	0.74	9.90E+02	8.90E+04
TFE731-5	Garrett	3.34	--	--	2.00E+04
J85-5H	GE	0.00	0.52	2.65E+02	1.71E+04
J85-21	GE	0.00	0.51	3.03E+02	2.22E+04
J85--7	GE	0.00	0.45	1.79E+02	1.27E+04
GE90-B4	GE	8.40	--	--	3.89E+05
GE90-90B	GE	8.40	3.40	7.56E+03	4.01E+05
FI01--02	GE	--	1.40	2.02E+03	1.37E+05
FI00-229	GE	--	1.19	1.38E+03	1.29E+05
FI 10-I00	GE	0.87	1.18	1.77E+03	1.27E+05
F414-400	GE	--	--	--	9.79E+04
F404-FID	GE	--	0.88	--	4.45E+04
F404-402	GE	0.27	0.88	1.04E+03	7.87E+04
F404-400	GE	0.34	0.88	9.89E+02	7.12E+04
F118--00	GE	--	1.18	1.45E+03	8.45E+04
F110--29	GE	0.76	1.18	1.79E+03	1.29E+05
CF700	GE	--	0.94	3.48E+02	2.00E+04
CF6-80C2	GE	5.05	2.69	4.31E+03	2.70E+05
CF6-50	GE	4.31	2.67	3.96E+03	2.34E+05
CF34-8D3	GE	5.00	1.32	1.12E+03	5.97E+04
CF/TF-34	GE	--	1.24	7.58E+02	4.09E+04
HFX-01	Honda	3.90	0.71	1.92E+02	8.01E+03
HF118	Honda	--	--	--	7.43E+03
TFE1042-70	Honey	0.40	0.59	6.17E+02	4.11E+04
ATF3-6A	Honey	2.80	0.85	5.10E+02	2.42E+04
V2533-A5	IAE	4.40	1.60	2.50E+03	1.47E+05
V2528-D5	IAE	4.70	--	--	1.25E+05
V2522-A5	IAE	4.90	1.60	2.36E+03	9.79E+04
TF-40	IHI	--	2.90	7.67E+02	3.25E+04
F3-30	IHI	0.90	0.56	3.40E+02	1.64E+04
F-3	IHI	--	2.01	2.08E+02	1.65E+04
K--5	IL	0.00	0.73	3.20E+02	1.47E+04
NK-86	KKBM	1.60	1.60	2.45E+03	1.28E+05
RD-35	Klimov	1.46	0.99	4.40E+02	2.16E+04
RD-33	Klimov	0.49	1.04	1.06E+03	8.14E+04
WP13F	LMC	0.00	--	--	6.47E+04
WP13A II	LMC	0.00	0.91	1.20E+03	6.59E+04
AL-7F	Lyulka	0.00	1.25	2.01E+03	8.82E+04
AL-31F	Lyulka	0.60	1.22	1.53E+03	1.07E+05
AL-21F	Lyulka	0.00	0.88	1.72E+03	1.10E+05
PW6124	PW	4.50			1.06E+02
PW500	PW	--	0.69	3.47E+02	1.33E+04
PW4098	PW	5.80	3.04	7.48E+03	4.36E+05
PW4084	PW	6.41	--	--	3.91E+05
PW4052	PW	5.00	--	--	2.31E+05
PW305	PW	4.30	0.97	4.72E+02	2.34E+04
PW306	PW	4.50	0.97	4.72E+02	2.54E+04
PW300	PW	4.50	--	--	2.11E+04
PW2037	PW	5.80	2.15	3.25E+03	1.70E+05
JT9D-59A	PW	4.90	2.46	4.15E+03	2.36E+05
JT9D	PW	5.00	2.43	3.91E+03	1.93E+05
JT8D--5A	PW	1.04	--	--	6.89E+04
JT8D	PW	1.10	--	--	6.23E+04
JT3D	PW	1.36	1.35	1.95E+03	8.01E+04
JT15D--B	PW	3.30	0.69	2.35E+02	9.79E+03
JT15D	PW	--	0.71	2.86E+02	1.33E+04
F135	PW	0.20	--	--	1.78E+05
F117--00	PW	6.00	2.15	3.22E+03	1.81E+05
F100-220	PW	0.70	1.18	1.45E+03	1.06E+05
F100--00	PW	0.69	--	--	1.05E+05
Viper 680	RR	0.00	0.74	3.79E+02	1.94E+04
Trent 970	RR	8.50	2.95	--	3.11E+05
Trent 895	RR	5.79	2.79	5.98E+03	4.25E+05
Trent 600	RR	8.00	2.47	4.72E+03	3.06E+05
Spey 807	RR	0.93	0.83	--	4.91E+04
RB211-882	RR	6.01	--	--	3.77E+05
RB211-535E	RR	4.30	--	--	1.78E+05
RB211-524B	RR	4.50	--	--	2.22E+05

Model	Manufacture	β	d	m	τ
RB211-22B	RR	5.00	2.15	4.17E+03	1.87E+05
RB.153-61	RR	--	--	--	5.23E+04
Pegasus 11-	RR	1.20	1.22	1.93E+03	1.06E+05
Pegasus	RR	--	1.22	--	9.56E+04
FJX-2	RR	--	0.36	4.54E+01	3.11E+03
FJ44-1,2	RR	--	0.53	2.02E+02	8.45E+03
F107/F112	RR	--	0.30	6.62E+01	3.11E+03
AE 3007A1P	RR	4.80	0.98	--	3.37E+04
Adour Mk	RR	0.75	0.56	--	3.74E+04
RB.193--2	RM	--	0.87	1.05E+03	4.52E+04
RB.162-81	RM	--	0.74	1.88E+02	2.48E+04
Olympus 593	RS	0.00	1.24	3.08E+03	1.69E+05
RD-41	Rybinsk	0.00	0.64	2.90E+02	4.02E+04
RD-38	Rybinsk	0.00	--	2.31E+02	3.19E+04
RD-36-	Rybinsk	0.00	--	2.01E+02	2.99E+04
RD-36-35FV	Rybinsk	--	--	--	2.84E+04
RD-36-35	Rybinsk	--	--	--	2.30E+04
NK-93	Samara	17.00	2.90	3.65E+03	1.77E+05
AL-55	Saturn	0.60	0.59	3.15E+02	2.16E+04
D-25VK	Soloviev	--	1.90	--	--
RD9B	Soyuz	0.00	0.67	7.00E+02	3.23E+04
RD3	Soyuz	0.00	1.40	3.11E+03	8.58E+04
R-79V-300	Soyuz	--	1.72	2.75E+03	1.52E+05
R-79	Soyuz	1.00	1.10	2.75E+03	1.52E+05
R-28V-300	Soyuz	0.00	1.01	--	6.57E+04
R-27V-300	Soyuz	0.00	1.01	1.35E+03	5.98E+04
R-27F2M-	Soyuz	0.00	1.01	1.50E+03	9.81E+04
R--95	Soyuz	0.00	0.91	9.90E+02	4.41E+04
R--3-300	Soyuz	0.00	0.91	1.21E+03	6.47E+04
R--1F-300	Soyuz	0.00	0.91	1.15E+03	5.64E+04
R-27-300	ST	--	--	--	4.90E+04
ALF5O2R-5	TL	5.70	--	5.83E+02	3.10E+04
FJ44	WR	3.28	--	--	8.45E+03
D-36	ZMKB	5.60	1.37	1.11E+03	6.37E+04
AL222-	ZMKB	1.19	0.81	5.20E+02	3.01E+04
V2500-A1	--	5.40	1.71	2.38E+03	1.11E+05
Trent 800	--	6.50	2.79	6.53E+03	4.09E+05
TFE731-20	--	--	1.00	4.01E+02	1.62E+04
TFE731-2	--	2.67	1.00	3.29E+02	1.56E+04
TFE731-2	--	2.66	1.02	2.84E+02	1.56E+04
TF41-A--B	--	--	1.02	1.59E+03	6.45E+04
TF39--	--	--	2.54	3.26E+03	1.82E+05
TF34--00	--	--	1.27	6.45E+02	4.03E+04
TF33-P-7	--	--	1.37	2.11E+03	9.34E+04
TF33-P-3	--	--	1.35	1.77E+03	7.56E+04
TF30-P--11	--	--	1.24	1.81E+03	1.12E+05
TBE-M2.0	--	--	--	4.21E+03	3.07E+05
TBE-M1.6	--	--	--	4.20E+03	3.14E+05
TBE-2.4	--	--	--	4.35E+03	2.91E+05
Tay 620	--	3.04	1.52	1.44E+03	6.16E+04
RD-41	--	--	0.64	2.90E+02	4.02E+04
RB211-524H	--	4.10	2.19	4.31E+03	2.70E+05
RB.162-31	--	--	--	--	2.40E+04
RB.162	--	--	0.66	--	2.45E+04
RB.145	--	0.00	0.53	--	1.62E+04
JT9D-3A	--	--	2.43	3.90E+03	1.93E+05
JT8D-7B	--	--	1.14	--	6.45E+04
JT8D-217	--	1.74	1.43	2.01E+03	9.27E+04
JT8D--1	--	--	1.09	1.50E+03	6.67E+04
JT3-D-7	--	--	1.34	1.95E+03	8.45E+04
JT3D-3B	--	--	1.35	1.95E+03	8.01E+04
J79--7	--	0.00	0.99	1.75E+03	7.93E+04
J75-P--7	--	0.00	1.09	2.66E+03	1.09E+05
J69-T-25	--	0.00	0.57	1.65E+02	4.56E+03
J60-P-3	--	0.00	0.59	2.09E+02	1.33E+04
J58-P	--	0.00	--	--	1.45E+05
J57-P-43WB	--	0.00	0.99	1.76E+03	4.98E+04
J57-P-23	--	0.00	1.02	2.34E+03	7.12E+04
GE4	--	--	2.29	6.01E+03	3.07E+05
GE21J11B14	--	--	1.88	--	2.89E+05
FJ44-2	--	3.28	0.60	2.03E+02	1.02E+04
FJ44--	--	--	0.53	2.02E+02	8.45E+03
F117-PW--	--	5.90	2.15	--	1.85E+05
F108-CF--00	--	--	1.83	2.09E+03	9.62E+04
F107-WR--0I	--	--	0.30	6.40E+01	2.82E+03
F103--01	--	--	2.19	3.98E+03	2.30E+05
CFM56-5C2	--	6.60	1.84	--	1.39E+05
CF34-3B	--	--	1.24	7.58E+02	4.10E+04
ALF502R-6	--	--	1.27	6.24E+02	3.34E+04

Model	Manufacture	d	m	P_{engine}
D-25V	Aviadvigatel	1.086	1325	4.05E+06
Smart	DaimlerChrysler	–	66	4.00E+04
CT7-5A	GE	0.737	355	1.29E+06
T700-700	GE	0.635	198	1.21E+06
2706	Hirth	–	31	4.85E+04
F 30	Hirth	–	36	7.08E+04
NK-12MV	KKBM	1.15	2900	1.10E+07
TV3-117VMA	Klimov	0.65	560	1.86E+06
T800-801	LHTEC	0.5501	149.7	1.17E+06
L 2400EFI turbo	Limbach	–	77	7.46E+04
PT6A-27	PW	0.483	149	5.07E+05
PT6A-68	PW	0.483	259.5	1.19E+06
PW150A	PW	0.767	690	3.78E+06
PW206A	PW	0.5	108	4.77E+05
AI-14RA	PZL	–	200	1.91E+05
K-9	PZL	–	580	8.60E+05
912 UL	Rota	–	59	5.96E+04
250-C40B	RR	0.577	71.5	3.13E+05
Gem 42	RR	0.575	183	7.46E+05
T56-15	RR	0.686	828	3.42E+06
EJ22	Subaru	–	119	1.19E+05
TSIOL-550-C	TCM	–	188.4	2.61E+05
O-360-A	Tetron Lycoming	–	120	1.34E+05
Arrius 1D	Turbomeca	–	111	3.13E+05
416	VAZ	–	125	1.34E+05
Twinpack	Wankel Rotary	–	119	1.10E+05
D-127	ZMKB	1.4		1.07E+07
D-136	ZMKB Progress	1.382	1077	7.46E+06
PT6A-42	–	0.4826	177.3576	6.34E+05
PT6A-45R	–	0.4826	196.8624	8.93E+05
T400-CP-400	–	1.1049	324.7776	1.34E+06
T406-AD-400	–	0.6223	442.26	4.59E+06
T53-L-13	–	0.5842	249.0264	1.04E+06
T55-L-11	–	0.61722	303.912	2.80E+06
T56-A-15	–	1.13284	838.2528	3.42E+06
T56-A-7	–	1.03886	831.4488	2.82E+06
T58-100	–	0.5461	151.956	1.12E+06
T64-100	–	0.51308	326.592	3.23E+06
T76-G-10	–	0.68834	157.8528	5.33E+05

* Vehicles with more than one power plant type, included as nT_{engine}

AS: Armstrong Siddeley
TL: Textron Lycoming
ST: Soyuz Tumanskiy
RM: RR/MTU
RS: RR/SNECMA
WR: Williams Rolls
TCM: Teledyne Continental Motors

Note: tabulated data found in this section are compiled from various references [7,9,10,8,13,14,28,29].

A.4 Sample Design Output Results

A.4.1 With Partial Neural Estimation

Airframe	m	M	Z	$X_{takeoff}$	$X_{landing}$	$T_{equipped}$	T_{result}	Condition	ε
Rafale	2.45E+04	1.80	16765	600	*600*	1.61E+05	1.56E+05	$T_{optimal}$	2.6%
CRJ200	2.15E+04	0.74	12500	1527	1423	7.46E+04	4.98E+04	$T_{takeoff}$	33.2%
737-900	7.90E+04	0.82	12500	2439	1662	2.21E+05	[illegible]	T_{mach}	15.7%
IL-214	5.50E+04	0.75	12000	*1000*	*980*	1.90E+05	1.54E+05	$T_{takeoff}$	18.7%
MiG-23	1.47E+04	2.35	18500	500	750	1.16E+05	1.03E+05	$T_{optimal}$	11.2%
Mako	9.40E+03	1.50	14400	450	750	8.18E+04	3.41E+04	$T_{takeoff}$	58.3%
An-72	2.75E+04	0.56	*10210*	620	420	1.16E+05	1.29E+05	$T_{takeoff}$	-11.7%
An-74	3.65E+04	0.65	10210	930	465	1.16E+05	1.15E+05	$T_{takeoff}$	1.0%
VJ-101C	6.60E+03	1.30	12000	0	0	8.86E+04	7.12E+04	$T_{takeoff}$	19.6%
Jas-39A	1.40E+04	1.00	15239	800	600	7.32E+04	3.87E+04	$T_{takeoff}$	47.1%
F-8 IIM	1.89E+04	2.20	18000	630	900	1.24E+05	1.27E+05	$T_{optimal}$	-2.9%
Legacy B	2.00E+04	0.79	11887	1759	813	8.00E+04	5.16E+04	T_{mach}	14.0%

Italics: estimated values

Gray entries: error resulted from the calculation of T_{mach}

Airframe	n		T_{engine}			W_{engine}			β			d			Engine
	Actual	Result	Actual	Result	Error	Actual	Result	Error	Actual	Result	Error	Actual	Result	Error	
Rafale	2	2	—	1.11E+05	—	—	1.98E+03	—	—	0.75	—	—	1.19	—	M88-3
CRJ200	2	1	[illegible]	[illegible]	33.5%	[illegible]	[illegible]	40.1%	—	0.50	—	1.24	0.94	24.2%	CF34-3B
737-900	2	2	1.21E+05	1.02E+05	15.7%	2.38E+03	1.83E+03	23.1%	5.1	5.60	9.8%	1.55	1.71	10.7%	CFM56-7B27s
IL-214	2	2	1.05E+05	8.50E+04	18.7%	—	1.55E+03	—	5	5.60	12.0%	—	1.39	—	CFM56-3
MiG-23	1	1	—	1.56E+05	—	—	2.71E+03	—	—	0.76	—	—	1.10	—	R-35-300
Mako	1	1	8.90E+04	3.75E+04	57.8%	9.90E+02	7.82E+02	21.0%	0.4	0.75	87.5%	0.74	0.61	18.2%	EJ200
An-72	2	2	6.37E+04	7.12E+04	11.8%	1.11E+03	1.33E+03	19.8%	5.6	5.60	0.0%	1.37	1.37	0.0%	D-36
An-74	2	2	—	6.31E+04	—	—	1.20E+03	—	—	5.60	—	—	1.37	—	D-36 2A
VJ-101C	6	1	1.62E+04	7.83E+04	382.6%	—	1.44E+03	—	0	0.40	—	0.53	0.92	74.9%	RB.145
Jas-39A	1	1	7.12E+04	4.26E+04	40.2%	9.89E+02	8.64E+02	12.7%	0.34	0.93	173.4%	0.88	0.78	11.4%	F404-400
F-8 IIM	2	1	—	1.65E+05	—	—	2.90E+03	—	—	0.76	—	—	1.10	—	—
Legacy B	2	1	3.67E+04	5.67E+04	68.3%	—	1.09E+03	—	4.8	0.00	100.0%	0.98	0.95	2.5%	AE 3007A1P

Gray entries: Values based on different number of engines

A.4.2 Without Neural Estimation

Airframe	m	M	Z	$X_{takeoff}$	$X_{landing}$	$T_{equipped}$	T_{result}	Condition	ε
J-8 II	1.53E+04	2.20	20200	670	1000	1.20E+05	1.02E+05	$T_{optimal}$	14.6%
J-7E	9.10E+03	2.35	17500	700	700	5.88E+04	5.72E+04	$T_{takeoff}$	2.7%
Jaguar	1.57E+04	1.50	13716	1250	680	6.80E+04	4.01E+04	$T_{takeoff}$	41.1%
GR. Mk 7	8.70E+03	0.98	15600	0	0	9.62E+04	9.39E+04	$T_{optimal}$	2.5%
T-4	7.50E+03	0.91	14815	655	704	2.98E+04	2.89E+04	$T_{takeoff}$	3.0%
Su-25	1.76E+04	0.80	7000	500	650	8.03E+04	7.34E+04	$T_{optimal}$	8.7%
Falcon 900	2.52E+04	0.87	15500	1580	720	5.76E+04	3.56E+04	T_{mach}	-45.5%
767-200ER	1.56E+05	0.80	11550	2071	1372	4.09E+05	3.93E+05	$T_{takeoff}$	4.0%
777-200ER	2.63E+05	0.84	13137	3030	1836	7.65E+05	7.29E+05	T_{mach}	3.4%
A340-200	2.75E+05	0.86	11887	3017	1890	5.05E+05	5.93E+05	$T_{takeoff}$	-17.4%

Gray entries: error resulted from the calculation of T_{mach}

Airframe	n		T_{engine}			W_{engine}			β			d			Engine
	Actual	Result	Actual	Result	Error	Actual	Result	Error	Actual	Result	Error	Actual	Result	Error	
J-8 II	2	1	---	1.23E+05	---	---	2.13E+03	---	---	0.75	---	---	1.19	---	WP13A
J-7E	1	1	6.47E+04	5.83E+04	10.0%	—	1.12E+03	—	0	0.00	—	—	0.95	—	WP13F
Jaguar	2	1	3.74E+04	4.41E+04	18.0%	---	8.88E+02	---	0.75	0.75	0.0%	0.56	0.69	24.3%	Adour Mk 811
GR. Mk 7	1	1	1.06E+05	1.03E+05	2.5%	1.93E+03	1.85E+03	4.3%	1.2	1.20	0.0%	1.22	1.22	0.0%	Pegasus 11-61
T-4	2	1	1.34E+04	2.30E+04	40.2%	3.40E+02	5.45E+02	60.4%	0.9	0.40	0.0%	0.56	0.60	6.6%	F3-30
Su-25	2	1	---	1.62E+05	---	---	2.80E+03	---	---	1.20	---	---	1.19	---	R-195
Falcon 900	3	1	---	9.41E+04	---	---	1.70E+03	---	---	0.49	---	---	0.86	---	---
767-200ER	2	2	—	2.16E+05	—	—	3.68E+03	—	—	5.05	—	—	2.45	—	—
777-200ER	2	2	4.25E+05	4.01E+05	5.7%	5.98E+03	6.68E+03	11.6%	5.79	5.79	0.0%	2.79	2.79	0.0%	Trent 895
A340-200	4	2	1.39E+05	3.26E+05	134.9%	---	5.46E+03	---	6.6	5.79	12.3%	1.84	2.69	46.6%	CFM56-5C2

Gray entries: Values based on different number of engines

A.5 Type U and Type C Engine Modeling

Short takeoff performances of several airplanes are simulated based on the linear assumption of lift increase as a function of thrust, as in equation 12. For upper engine configurations, flight data of the Aska were used and extrapolated through a family of lines as follows.

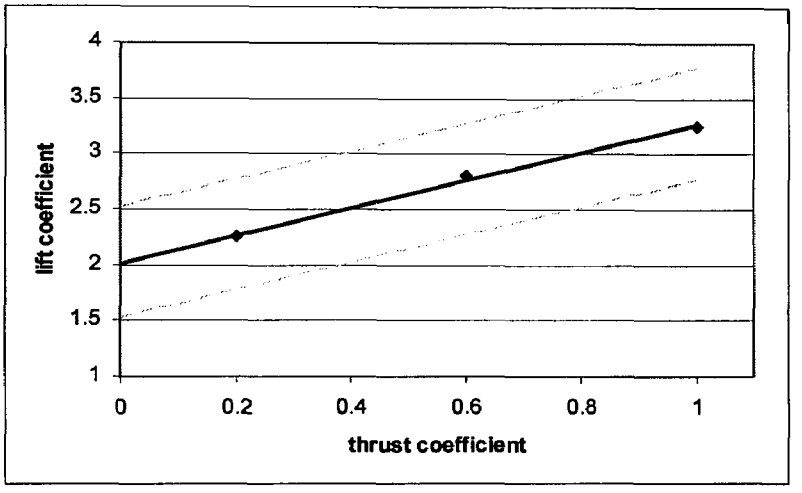

Reproduction of the Aska at 10° angle of attack from flight data [15]

Similarly, vehicles with type C engine configuration are modelled in the figure below, for the performances of short takeoff.

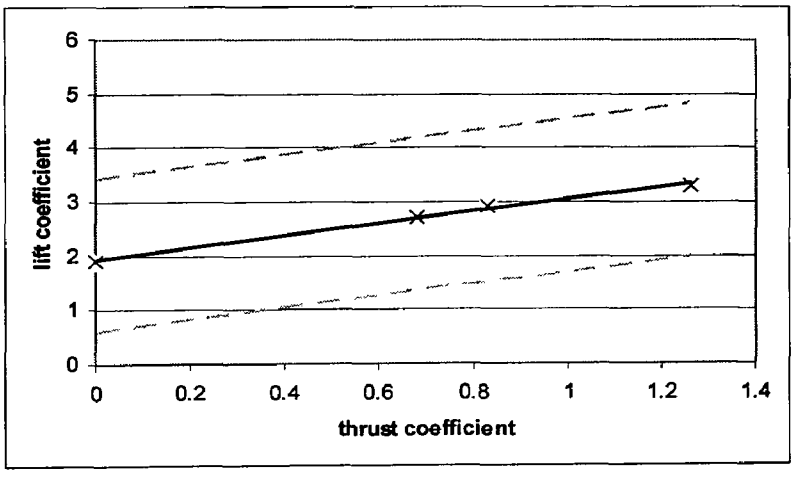

Reproduction of wind tunnel experimentation data from literature [16]

The above models are used to simulate takeoff of a number of vehicles. A thrust recovery factor of 0.71 compensates for losses through aerodynamic deflection of exhaust [26]. This is applied to both *U* and *C* type takeoffs. The table below shows the calculated thrust requirements derived from the above V/STOL models. The idealisation of the above takeoff models via linear interpolation has yielded significant underestimations of the actual thrust.

Airframe	m	$X_{takeoff}$	$X_{landing}$	$T_{equipped}$	$T_{takeoff}$	ε_1	$T_{deflect}$	ε_2	Λ
An-72	3.30E+04	620	420	1.15E+05	1.36E+05	-18.1%	3.24E+04	71.8%	Upper
An-74	3.65E+04	930	465	1.15E+05	1.02E+05	10.9%	3.58E+04	68.8%	Upper
YC-15	7.01E+04	610	610	2.56E+05	3.00E+05	-17.2%	6.88E+04	73.1%	Conventional
YC-14	7.71E+04	571.5	610	4.09E+05	---	—	---	—	Upper
C-17A	2.65E+05	2124	823.5	6.48E+05	9.41E+05	-45.2%	2.60E+05	59.8%	Conventional
Aska	3.87E+04	578	408	1.52E+05	7.83E+04	48.5%	3.80E+04	75.0%	Upper
777-200ER	2.98E+05	3030	1630	7.47E+05	7.24E+05	3.1%	2.92E+05	60.9%	Conventional
A380-800	5.60E+05	2050	2900	1.28E+06	1.59E+06	-24.4%	5.49E+05	57.1%	Conventional
A340-200	2.75E+05	3017	1890	5.00E+05	5.39E+05	-8.0%	2.70E+05	46.0%	Conventional

$$\varepsilon_1 = (T_{equipped} - T_{takeoff}) / T_{equipped}$$

$$\varepsilon_2 = (T_{takeoff} - T_{deflect}) / T_{takeoff}$$

There is no reference thrust rating for the YC-14, power rated research vehicle.

Results of upper and lower type takeoff modeling

A.6 Results of Various Neural Regression of Stall

The following compares three neural network estimations of stall, composed of different sets of primary input parameters:

Airframe	Actual	$neural(W, M, X_{takeoff})$	ε	$neural(W, X_{takeoff}, S)$	ε	$neural(W, X_{takeoff})$	ε
RAH-66	0.0	0.0	0.0%	0.0	0.0%	0.	0.0%
Yak-38	0.0	0.0	0.0%	0.0	0.0%	0.	0.0%
GR. Mk 7	0.0	0.0	0.0%	0.0	0.0%	0.	0.0%
RJ100	48.9	48.9	0.0%	48.3	1.3%	77.	58.9%
MiG-31	72.5	72.5	0.0%	77.7	7.1%	77.	7.1%
767-200ER	63.4	63.4	0.0%	63.0	0.7%	63.	0.7%
Sea Harrier	—	45.8	—	45.8	—	45.	—
777-200ER	65.1	68.4	5.2%	68.4	5.2%	68.	5.2%
CRJ200	69.4	54.4	21.6%	54.4	21.6%	54.	21.6%
737-900	72.5	56.5	22.1%	63.0	13.2%	54.	24.9%
IL-214	69.4	48.9	29.6%	47.8	31.2%	47.	31.2%
Average			7.1%		7.3%		13.6%

It is noted that the second neural network is comparatively accuracy with respect to the first network. Since the parameter S is not a primary input value, it may be necessary to first estimate S, e.g., via equation 8. However, successive estimations of parameters may lead to possible error amplification towards the prediction of v_{stall}. The third neural network is unable to distinguish the stall characteristics of regional jets from military vehicles from the results of RJ100 and MiG-31, in which this is provided by the parameters M or S.